LES–Lagrangian particle method for turbulent reactive flows based on the approximate deconvolution model and mixing model

Tomoaki Watanabe[a,b,1,*], Yasuhiko Sakai[a], Kouji Nagata[a], Yasumasa Ito[a], Toshiyuki Hayase[c]

[a] *Department of Mechanical Science and Engineering, Nagoya University, Nagoya 464-8603, Japan*
[b] *Research Fellow of the Japan Society for the Promotion of Science*
[c] *Department of Mechanical Science and Engineering, Tohoku University, Sendai 980-0812, Japan*

Abstract

We propose a numerical method for turbulent reactive flows using a large eddy simulation (LES) based on the approximate deconvolution model (ADM). LES based on the ADM is combined with a Lagrangian notional particle (LP) method for computing reactive flows without using models for chemical source terms. In the LP method, values of scalars are assigned to each particle. The evolutions of Lagrangian particles in physical and scalar composition spaces are modeled by using the mixing model for molecular diffusion and the resolved velocity field of LES. We also propose a mixing model using a mixing volume concept, in which the mixing timescale is determined by relating the decay of scalar variance in the mixing volume to the scalar dissipation rate. The LES–LP method based on the ADM and the mixing model is applied to a planar jet with a second-order reaction for testing the numerical

*Corresponding author (+81-052-789-4487)
Email address: watanabe.tomoaki@c.nagoya-u.jp (Tomoaki Watanabe)

method. The statistics obtained by the LES–LP method are compared with the direct numerical simulation data. The results show that the evolutions of Lagrangian particles are well modeled in the LES–LP method by using the resolved velocity and the mixing model, and the LES–LP method can accurately predict the statistical properties of reactive scalars. The mixing timescale depends on the distance among the Lagrangian particles. It is also shown that the present mixing model can implicitly take into account the effect of distance among the particles by adjusting the mixing timescale without using any model parameters.
Keywords: Large Eddy Simulation, Mixing, Chemical Reaction, Jet

1. Introduction

Turbulent mixing with chemical reactions can be observed in engineering and environmental flows (e.g., in chemical reactors and for pollutants emitted into the atmosphere). Large eddy simulation (LES) has been one of the most common tools to predict mixing and scalar transfer in turbulent flows, and it is expected to be applicable to engineering and environmental flows. In LES, velocity and scalar fields are divided into large-scale and small-scale parts by a filtering procedure. LES resolves large-scale features in flows, whereas the effects of unresolved small-scale [subgrid scale (SGS)] features have to be modeled. In LES of turbulent reactive flows, SGS scalar fluctuations have to be modeled to close the filtered reaction source terms, which appear in an unclosed form in the filtered scalar transport equations.[1] LES of turbulent reactive flows using models for the SGS scalar fluctuations has been developed in several studies.[2,3,4] However, LES is often combined with another

numerical method to simulate reactive scalars [e.g., conditional moment closure[5] and the probability density function (PDF) method[6,7]] because it is difficult to model the contribution of SGS scalar fluctuations to the filtered reaction source terms.

Most of LES for reactive flows has been developed based on the Smagorinsky model[8] (the dynamic Smagorinsky model[9]) for the SGS Reynolds stress and the gradient diffusion model for the SGS scalar flux. The gradient diffusion model is widely used with a dynamic procedure to determine the SGS turbulent Schmidt (Prandtl) number.[10] SGS models used in LES can be classified into two main types: eddy viscosity models (e.g., the Smagorinsky model, the dynamic Smagorinsky model, and the structure-function model[11]), and models based on the reconstruction of the information in small scales from a resolved field (e.g., the scale similarity model[12]). Recently, Stolz and Adams proposed the approximate deconvolution model[13] (ADM), in which the information in the small scales is approximately reconstructed by using an approximate deconvolution filter. LES based on the ADM has been applied to various turbulent flows.[14,15,16,17] The ADM has some advantages over the Smagorinsky model or the dynamic Smagorinsky model. It is well known that the Smagorinsky model is too dissipative.[16] The dynamic Smagorinsky model overcomes some of problems in the Smagorinsky model by dynamically determining the model parameter. However, the procedure to determine the model parameter often includes spatial averaging to prevent numerical instability.[18] Spatial averaging might be inadequate for intermittent flows, which consist of turbulent, non-turbulent, and transition regions,[19] because the SGS eddy viscosity changes between turbulent and

non-turbulent regions.[20] It was also reported that the eddy viscosity model can reduce the effective Reynolds number of the flow.[21] Some of these problems relating to the eddy viscosity model do not exist in LES based on the ADM. The ADM can be applied to both turbulent and non-turbulent flows without adjusting the model.[16] In LES based on the ADM, the flow and scalar fields can be divided into three scales: a filtered scale, for which the spatial filtering procedure has no explicit effects, a subfilter scale, which can be represented on a computational grid of LES but is removed or suppressed by the filter, and a subgrid (unresolved) scale, which cannot be represented on the computational grid.[22] The filtered and subfilter scales can be collectively referred to as the resolved scale. The ADM can reconstruct well the subfilter scale although the SGS is implicitly modeled by a relaxation term, which emulates the dissipations in the SGS.

In turbulent reactive flows, mixing at the molecular level often controls chemical reaction rates.[23] Therefore, the effects of SGS scalar fluctuations on chemical reactions should be accurately modeled in LES. However, in the ADM, it is difficult to model these effects because the ADM can reconstruct only the subfilter scales. To overcome the difficulty in modeling the chemical source terms by the ADM, we combine the LES based on the ADM with the representation of scalar fields by Lagrangian notional particles. Values of reactive scalars are assigned to each particle. This numerical method is referred to as a LES–Lagrangian particles (LES–LP) method hereafter. The LES is often combined with the filtered density function (FDF) method,[24] in which Lagrangian stochastic particles are used for solving the governing equation for the FDF. The present method is derived based on the Lagrangian de-

scription of scalar transport equations rather than the FDF. Furthermore, the FDF method has been developed based on the eddy viscosity model although we use the ADM as the SGS model in the LES–LP methods. In the LES–LP method, the LES based on the ADM is used for computing the resolved velocity and nonreactive scalar fields whereas the reactive scalar fields are computed by using the Lagrangian particles which evolve according to the scalar transport equations. Because the reactive scalars are treated by the Lagrangian particles, the models for the reaction source terms are not required in the LES. Because of the difficulty in accurately computing the spatial scalar derivative using the Lagrangian particles, the molecular diffusion term is modeled by a mixing model using multiple Lagrangian particles.[1,25] The mixing model requires to specify a mixing timescale of the model among the Lagrangian particles. The mixing timescale is often determined using the ratio of the mechanical timescale to the scalar timescale.[1,25] However, it was reported that this ratio changes depending on the Reynolds number and the Schmidt number.[26] Therefore, this procedure to determine the mixing timescale includes adjusting a model parameter, which has a great influence on the numerical results. In this study, we also develop a mixing model based on a mixing volume concept, in which the mixing timescale is determined so that the mixing model decays scalar variance in the mixing volume according to the scalar dissipation rate. It is shown that the present model can implicitly take into account the effect of distance among mixing particles without adjusting any model parameters.

In Sec. 2, we describe the detail of the LES–LP method and the mixing model. The LES–LP method based on the ADM and the new mixing model

is applied to a planar jet with an isothermal second-order reaction A+B $\rightarrow$ P (Sec. 3) for testing the numerical method. The results of LES–LP simulation are compared with the previous direct numerical simulation (DNS) data[27,28] in Sec. 4 to demonstrate that the LES–LP method based on the ADM and the present mixing model is useful for predicting turbulent reactive flows.

2. LES–LP method based on the ADM and mixing model

2.1. Large eddy simulation based on the ADM

An incompressible fluid with a nonreactive passive scalar transfer is treated in the LES. The governing equations for velocity U_i and nonreactive passive scalar ψ are the continuity equations, the Navier–Stokes equations, and the transport equation for ψ:

$$\frac{\partial U_j}{\partial x_j} = 0, \tag{1}$$

$$\frac{\partial U_i}{\partial t} + \frac{\partial U_j U_i}{\partial x_j} = -\frac{\partial P}{\partial x_i} + \nu \frac{\partial^2 U_i}{\partial x_j \partial x_j}, \tag{2}$$

$$\frac{\partial \psi}{\partial t} + \frac{\partial U_j \psi}{\partial x_j} = D \frac{\partial^2 \psi}{\partial x_j \partial x_j}, \tag{3}$$

where P is the instantaneous pressure divided by the density ρ, ν is the kinematic viscosity, and D is the diffusivity coefficient relating to ψ. A spatial filtering operator G is defined by

$$\overline{f}(x,y,z) \equiv G * f \equiv \int_{-\infty}^{\infty}\int_{-\infty}^{\infty}\int_{-\infty}^{\infty} G(x-x', y-y', z-z') f(x', y', z') dx' dy' dz'. \tag{4}$$

The filtered equations can be obtained by applying the filter G to Eqs. (1), (2), and (3):

$$\frac{\partial \overline{U_j}}{\partial x_j} = 0, \tag{5}$$

$$\frac{\partial \overline{U_i}}{\partial t} + \frac{\partial \overline{U_j U_i}}{\partial x_j} = -\frac{\partial \overline{P}}{\partial x_i} + \nu \frac{\partial^2 \overline{U_i}}{\partial x_j \partial x_j}, \tag{6}$$

$$\frac{\partial \overline{\psi}}{\partial t} + \frac{\partial \overline{U_j \psi}}{\partial x_j} = D \frac{\partial^2 \overline{\psi}}{\partial x_j \partial x_j}. \tag{7}$$

In LES, these equations are solved to predict the filtered velocity $\overline{U_i}$ and the filtered scalar $\overline{\psi}$ by using models for the nonlinear term $\partial \overline{U_j U_i}/\partial x_j$ in Eq. (6) and the convective transport term $\partial \overline{U_j \psi}/\partial x_j$ in Eq. (7).

The ADM approximately reconstructs the unfiltered velocity and the unfiltered scalar value from the filtered quantities. For the filter G, the inverse filter G^{-1} is defined by the following relationship:

$$\overline{f} \equiv G * f, \tag{8}$$

$$f \equiv G^{-1} * \overline{f}. \tag{9}$$

An approximate deconvolution filter $Q_N \approx G^{-1}$ can be obtained by using the van Cittert deconvolution method:[13,29]

$$Q_N = \sum_{n=0}^{N_\mathrm{D}} (I - G)^n, \tag{10}$$

where I is the identity operator. Under the assumption that the filter G has the inverse operator G^{-1}, G^{-1} can be expanded as an infinite series of G. The approximate deconvolution filter can be obtained by truncating the expanded series at N_D as shown in Eq. (10). Stolz et al.[14] reported that when N_D is larger than 5, the results of LES are almost independent of N_D.

As the value of N_{D} increases, the computational cost for computing $Q_N * f$ becomes expensive because it requires N_{D} times computations of filter G. Therefore, the approximate deconvolution filter has often been computed by setting $N_{\mathrm{D}} = 5$ as in the previous studies.[14,15,16,17] The unfiltered value $\tilde{f}$ is approximately computed using Q_N:

$$\tilde{f} = Q_N * \overline{f}. \tag{11}$$

It should be noted that $\tilde{f}$ in LES contains the filtered and subfilter scales and does not contain the unresolved scale. In the ADM, $\tilde{U_i} = Q_N * \overline{U_i}$ and $\tilde{\psi} = Q_N * \overline{\psi}$ are used to model the nonlinear term and the convective transport term. Furthermore, to take into account dissipations in the unresolved scales, the relaxation terms $-\chi(I - Q_N * G) * \overline{U_i}$ and $-\chi(I - Q_N * G) * \overline{\psi}$ are added in the right-hand side of Eqs. (6) and (7), respectively. Here, χ is the relaxation parameter, which is often set to be constant or is dynamically determined according to the procedure proposed by Stolz et al.[14] The filtered Navier–Stokes equations and the filtered scalar transport equation based on the ADM are finally written as follows:

$$\frac{\partial \overline{U}_i}{\partial t} + \frac{\partial \overline{\tilde{U}_j \tilde{U}_i}}{\partial x_j} + \frac{\partial \overline{P}}{\partial x_i} - \nu \frac{\partial^2 \overline{U}_i}{\partial x_j \partial x_j} = -\chi(I - Q_N * G) * \overline{U}_i, \tag{12}$$

$$\frac{\partial \overline{\psi}}{\partial t} + \frac{\partial \overline{\tilde{U}_j \tilde{\psi}}}{\partial x_j} - D \frac{\partial^2 \overline{\psi}}{\partial x_j \partial x_j} = -\chi(I - Q_N * G) * \overline{\psi}. \tag{13}$$

For the low-pass filter G, the composite filter $(Q_N * G)$ becomes the low-pass filter whose cut-off is slightly smaller than that of G.[30] Thus, the relaxation terms remove the energy in the scales close to the smallest scales represented by the computational grid. Therefore, the explicit spatial low-pass filter,

which removes the small-scale energy, can be used instead of the relaxation terms.[30]

2.2. Lagrangian particle method

The reactive scalars are computed by using Lagrangian notional particles. LES based on the ADM computes $\overline{U_i}$ and $\overline{\psi}$. We consider passive scalar quantities $\mathbf{\Phi} = (\phi_1, \ldots, \phi_\alpha, \ldots, \phi_{N_\mathrm{S}})$, where N_S is the number of scalar quantities. The scalar transport equation for ϕ_α is assumed to be given by

$$\frac{\partial \phi_\alpha}{\partial t} + \frac{\partial U_j \phi_\alpha}{\partial x_j} = D_\alpha \frac{\partial^2 \phi_\alpha}{\partial x_j \partial x_j} + S_\alpha(\mathbf{\Phi}), \tag{14}$$

where D_α is the diffusivity coefficient for ϕ_α and S_α is the reaction source term for ϕ_α, which is a function of $\mathbf{\Phi}$.

We introduce the Lagrangian particles whose state is represented by the position $\mathbf{x}^{(n)}$ and the scalar quantities $\mathbf{\Phi}^{(n)} = (\phi_1^{(n)}, \ldots, \phi_\alpha^{(n)}, \ldots, \phi_{N_S}^{(n)})$. Here, n is used to identify the particle, and $n = 1 \ldots N_\mathrm{P}$, where N_P is the number of particles. The instantaneous value of ϕ_α at the particle position $\mathbf{x}^{(n)}$ is represented by $\phi_\alpha^{(n)}$. Under Eq. (14), the Lagrangian particles evolve in the physical ($\mathbf{x}$) and scalar composition ($\mathbf{\Phi}$) spaces according to the following equations:

$$\frac{d\mathbf{x}^{(n)}}{dt} = \mathbf{U}(\mathbf{x}^{(n)}, t), \tag{15}$$

$$\frac{d\phi_\alpha^{(n)}}{dt} = \left[D_\alpha \frac{\partial^2 \phi_\alpha}{\partial x_j \partial x_j} \right]^{(n)} + S_\alpha(\mathbf{\Phi^{(n)}}). \tag{16}$$

Here, the first term on the right-hand side of Eq. (16) represents the effect of molecular diffusion on $\phi_\alpha^{(n)}$, and cannot be explicitly expressed by $\mathbf{\Phi}^{(n)}$. In contrast, the second term, which is the reaction source term for $\phi_\alpha^{(n)}$, is

calculated from $\mathbf{\Phi}^{(n)}$ because S_α is represented as a function of $\mathbf{\Phi}$. In the LES–LP method, these equations are modeled using the unfiltered (resolved) velocity and the mixing model:

$$\frac{d\mathbf{x}^{(n)}}{dt} = \tilde{\mathbf{U}}(\mathbf{x}^{(n)}, t), \tag{17}$$

$$\frac{d\phi_\alpha^{(n)}}{dt} = \left[\frac{d\phi_\alpha^{(n)}}{dt}\right]_{\mathrm{mix}} + S_\alpha(\mathbf{\Phi^{(n)}}). \tag{18}$$

$\tilde{\mathbf{U}}(\mathbf{x}^{(n)}, t)$ in Eq. (17) can be obtained by interpolating $\tilde{\mathbf{U}}(\mathbf{x}, t)$ in LES on the particle position $\mathbf{x}^{(n)}$. The first term in Eq. (18) represents the effect of molecular diffusion modeled by the mixing model, and $[*]_{\mathrm{mix}}$ represents that the quantity is related to the mixing model. Unlike the exact equations for $\mathbf{x}^{(n)}$ and $\mathbf{\Phi}^{(n)}$, the modeled equations do not contain the unresolved velocity in the evolution of $\mathbf{x}^{(n)}$. Turbulent diffusion is mainly caused by the velocity related to large-scale energy-containing eddies.[31] Therefore, as long as $\tilde{\mathbf{U}}$ contains the large-scale contributions, most of turbulent diffusion is taken into account by Eq. (17). Similar to the relaxation term in LES, the dissipation of $\mathbf{\Phi}^{(n)}$ in the unresolved scale has to be included, and in the LES–LP method, this is implemented in the mixing model, whose detail is explained in the next subsection.

2.3. Mixing model for molecular diffusion

2.3.1. Mixing model based on mixing volume (mixing volume model)

The effect of molecular diffusion on $\mathbf{\Phi}^{(n)}$ is modeled by the interaction of particle n with other multiple particles. Here, we introduce the particles-interaction mixing model based on a mixing volume concept, which is referred to as the mixing volume model. For the particle n, the particles in a mixing

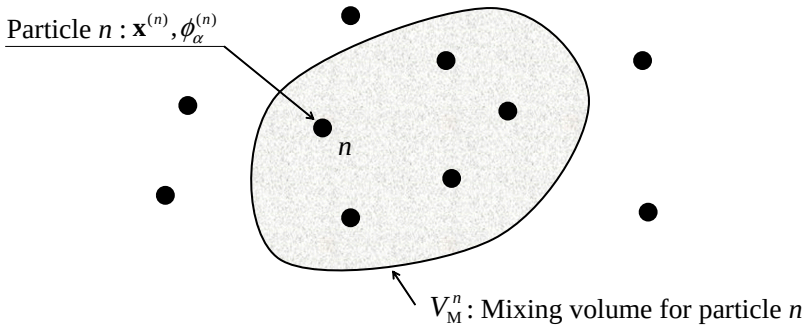

Figure 1: Schematic of particles around particle n and mixing volume V_{M}^n for the particle n. The particles in V_{M}^n are used to model the effect of molecular diffusion on $\phi_\alpha^{(n)}$.

volume V_{M}^n are used for computing the change in $\mathbf{\Phi}^{(n)}$ due to molecular diffusion. The molecular diffusion is modeled by the interaction between the particles, which changes scalar values of particles in V_{M}^n. Figure 1 shows the schematic of the particles around the particle n and the mixing volume V_{M}^n. The mixing volume is defined for the particle n as the space in which the particle n and all of particles used for the mixing with the particle n are contained. The mixing volume is determined for each particle. We do not confine the size and shape of V_{M}^n, and an arbitrary V_{M}^n can be used in the mixing volume model. A different mixing volume can be used for different particles. In practice, after particles which participate in the mixing event with the particle n are determined, the mixing volume V_{M}^n is determined so that those particles are involved in V_{M}^n. It is also possible to determine the mixing volume by dividing the computational domain into several grid cells. The grid cell in which the particle (n) is located can be used as V_{M}^n. The arbitrarity for determining the mixing volume can be used for improving the mixing volume model. The mixing is modeled by the interaction among

particles. Therefore, how many and which particles are located in the mixing volume are the most important in the mixing volume model rather than its shape. Here, we consider the IEM-type mixing scheme,[32] for which the change in $\phi_\alpha^{(n)}$ can be mathematically represented. For the particles inside the mixing volume, the change in $\phi_\alpha^{(n)}$ due to molecular diffusion is modeled by

$$\left[\frac{d\phi_\alpha^{(n)}}{dt}\right]_{\rm mix} = \frac{1}{\tau_{\rm M}}\left(\langle\phi_\alpha|V_{\rm M}^n\rangle - \phi_\alpha^{(n)}\right), \tag{19}$$

where $\tau_{\rm M}$ is a mixing timescale of the mixing model, which has to be specified for modeling the effect of molecular diffusion, and $\langle\phi_\alpha|V_{\rm M}^n\rangle$ is the average of ϕ_α of the particles in $V_{\rm M}^n$, which is defined by using the kernel function $G_n(\mathbf{x}^{(m)})$:

$$\langle\phi_\alpha|V_{\rm M}^n\rangle \equiv \frac{\sum_{m=1}^{N_{\rm P}} G_n(\mathbf{x}^{(m)})\phi_\alpha^{(m)}}{\sum_{m=1}^{N_{\rm P}} G_n(\mathbf{x}^{(m)})}, \tag{20}$$

$$G_n(\mathbf{x}^{(m)}) = \begin{cases} 1 & \text{If } \mathbf{x}^{(m)} \text{ is in mixing volume } V_{\rm M}^n \\ 0 & \text{otherwise} \end{cases}. \tag{21}$$

Equation (19) is applied for all particles in the mixing volume. Because $\langle\phi_\alpha|V_{\rm M}^n\rangle$ is the local mean value of ϕ_α in $V_{\rm M}^n$, the operator $\langle*|V_{\rm M}^n\rangle$ can be considered as the spatial low-pass filter based on $G_n(\mathbf{x}^{(m)})$. It should be noted that $\langle*|V_{\rm M}^n\rangle$ is independent of the low-pass filter used in LES, and is determined by $V_{\rm M}^n$. The relaxation term in Eq. (13) can be represented by $\chi(Q_N * G * \overline{\psi} - \overline{\psi})$, which is the similar form to the mixing volume model by Eq. (19). Here, $1/\chi$ corresponds to the mixing timescale $\tau_{\rm M}$, and the spatial low-pass filter $(Q_N * G)$ corresponds to $\langle*|V_{\rm M}^n\rangle$. Therefore, similar to the relaxation term, the mixing volume model by Eq. (19) dissipates the scalar fluctuations, and the intensity of the dissipation is controlled by $\tau_{\rm M}$.

For the filter $\langle *|V_{\rm M}^n\rangle$, the SGS scalar variance $\langle {\phi''}_\alpha^2|V_{\rm M}^n\rangle$, which is the local scalar variance in $V_{\rm M}^n$, can be defined by

$$\langle {\phi''}_\alpha^2|V_{\rm M}^n\rangle \equiv \langle \phi_\alpha^2|V_{\rm M}^n\rangle - \langle \phi_\alpha|V_{\rm M}^n\rangle^2. \tag{22}$$

Here, ${\phi''}_\alpha^{(n)} = \phi_\alpha^{(n)} - \langle \phi_\alpha|V_{\rm M}^n\rangle$ is satisfied for the definition of the filter operator $\langle *|V_{\rm M}^n\rangle$ by Eqs. (20) and (21). The mixing model causes the decay of $\langle {\phi''}_\alpha^2|V_{\rm M}^n\rangle$. In the LES using numerical filtering, which has a similar role to the relaxation term, the total energy-dissipation is represented by the sum of the contributions by the resolved scales and the numerical filter.[33] In the present mixing volume model, the mixing timescale is adjusted so that the mixing model dissipates the scalar fluctuations according to the total scalar dissipation rate. Although the unresolved velocity is not included in Eq. (17), the total dissipation contributed by both resolved and unresolved field is handled in the mixing model. Then, the mixing timescale can be obtained by relating the decay of $\langle {\phi''}_\alpha^2|V_{\rm M}^n\rangle$ with the scalar dissipation rate in $V_{\rm M}^n$ as described below. The time derivative of $\langle {\phi''}_\alpha^2|V_{\rm M}^n\rangle$ can be written as follows:

$$\begin{aligned}
\frac{d\langle {\phi''}_\alpha^2|V_{\rm M}^n\rangle}{dt} &= \frac{d\langle \phi_\alpha^2|V_{\rm M}^n\rangle}{dt} - \frac{d\langle \phi_\alpha|V_{\rm M}^n\rangle^2}{dt} \\
&= 2\left\langle \phi_\alpha \frac{d\phi_\alpha}{dt}\middle| V_{\rm M}^n\right\rangle - 2\langle \phi_\alpha|V_{\rm M}^n\rangle \left\langle \frac{d\phi_\alpha}{dt}\middle| V_{\rm M}^n\right\rangle .
\end{aligned} \tag{23}$$

Substituting Eq. (19) to Eq. (23) yields the temporal variation of $\langle {\phi''}_\alpha^2|V_{\rm M}^n\rangle$ by the mixing volume model, which is represented by

$$\begin{aligned}
\left[\frac{d\langle {\phi''}_\alpha^2|V_{\rm M}^n\rangle}{dt}\right]_{\rm mix} &= 2\left\langle \frac{\phi_\alpha}{\tau_M}\left(\langle \phi_\alpha|V_{\rm M}^n\rangle - \phi_\alpha\right)\middle| V_{\rm M}^n\right\rangle \\
&= -\frac{2}{\tau_{\rm M}}\left(\langle \phi_\alpha^2|V_{\rm M}^n\rangle - \langle \phi_\alpha|V_{\rm M}^n\rangle^2\right) \\
&= -\frac{2}{\tau_{\rm M}}\langle {\phi''}_\alpha^2|V_{\rm M}^n\rangle.
\end{aligned} \tag{24}$$

The mixing volume model by Eq. (19) decreases $\langle \phi''^2_\alpha | V_{\rm M}^n \rangle$ according to Eq. (24). Furthermore, the decay of $\langle \phi''^2_\alpha | V_{\rm M}^n \rangle$ is related to the filtered scalar dissipation rate by

$$\frac{d\langle \phi''^2_\alpha | V_{\rm M}^n \rangle}{dt} = -2\langle N_\alpha | V_{\rm M}^n \rangle, \tag{25}$$

$$N_\alpha = D_\alpha \frac{\partial \phi_\alpha}{\partial x_j} \frac{\partial \phi_\alpha}{\partial x_j}. \tag{26}$$

where N_α is the scalar dissipation rate for ϕ_α. From Eqs. (24) and (25), we can obtain the following expression for the mixing timescale:

$$\tau_{\rm M} = \frac{\langle \phi''^2_\alpha | V_{\rm M}^n \rangle}{\langle N_\alpha | V_{\rm M}^n \rangle}. \tag{27}$$

The mixing timescale of Eq. (27) is similar to the SGS mixing timescale,[34] and can be considered as the mixing timescale in the mixing volume. Although this mixing timescale of the mixing volume model is obtained for the IEM-type mixing scheme, it can be used in a different mixing scheme of the particles-interaction mixing model in which the same mixing timescale as the IEM-type mixing scheme is used.

Calculating of the mixing timescale using Eq. (27) from $\phi_\alpha^{(n)}$ is almost infeasible because of difficulty in estimating N_α from particles. Therefore, the nonreactive scalar computed in LES is used for calculating $\tau_{\rm M}$:

$$\tau_{\rm M} = \frac{\langle \psi''^2 | V_{\rm M}^n \rangle}{\langle N | V_{\rm M}^n \rangle}, \tag{28}$$

$$\langle \psi''^2 | V_{\rm M}^n \rangle = \langle \psi^2 | V_{\rm M}^n \rangle - \langle \psi | V_{\rm M}^n \rangle^2. \tag{29}$$

Here, $N = D(\partial\psi/\partial x_j)^2$ is the scalar dissipation rate for ψ, $\psi''^{(n)} = \psi^{(n)} - \langle \psi | V_{\rm M}^n \rangle$ is the scalar fluctuation in $V_{\rm M}^n$, and $\psi^{(n)}$ and $N^{(n)}$ can be obtained by interpolating ψ and N in LES on the particle position $\mathbf{x}^{(n)}$. For using Eq. (28), the molecular diffusivity should be equal for ψ and ϕ_α.

2.3.2. Implementation of mixing volume model in the LES–LP method

In the LES–LP method based on the ADM, τ_{M} is computed using the resolved values $\tilde{\psi} = Q_N * \overline{\psi}$ and $\tilde{N} = Q_N * \overline{N}$ instead of ψ and N. When the small-scale parts largely contribute to the scalar dissipation rate, the unresolved part of N is not negligible in the total N. However, the mixing timescale in Eq. (28) only requires the averaged value of N in V_{M}^n. The averaging procedure in the mixing volume is similar to applying the spatial low-pass filter, whose cut-off is related to the length scale of mixing volume. Therefore, when the length scale of V_{M}^n is larger than the LES grid size, using $\tilde{N}$ in Eq. (28) has a small influence on τ_{M} because the unresolved small-scale parts are removed by taking average in the mixing volume. The large mixing volume is related to a large distance among particles, which is caused by a small number of particles and a large computational domain. Using a small number of particles is also useful for reducing the computational cost. The locations of particles relative to each other are important in the mixing volume model. The unresolved velocity, which is neglected in Eq. (17), contributes to stirring of particles in unresolved small scales. When the distance between particles is larger than the unresolved scale in the LES, the unresolved velocity is expected to have very small influence on the mixing volume model because the movement of particles in unresolved small-scales hardly changes their locations relative to other particles.

The filtered scalar dissipation rate $\overline{N} = G * N$ can be divided into a large-scale part $N_{\mathrm{LS}} = D(\partial\overline{\psi}/\partial x_j)^2$ and a small-scale part N_{SS}:

$$\overline{N} = N_{\mathrm{LS}} + N_{\mathrm{SS}} = D\frac{\partial\overline{\psi}}{\partial x_j}\frac{\partial\overline{\psi}}{\partial x_j} + N_{\mathrm{SS}}. \tag{30}$$

Pierce and Moin[35] proposed the following model for N_{SS}:

$$N_{\mathrm{SS}} = -\overline{(U_j - \overline{U_j})(\psi - \overline{\psi})}\frac{\partial \overline{\psi}}{\partial x_j}. \tag{31}$$

Then, by using Q_N, the resolved scalar dissipation rate $\tilde{N}$ can be estimated from $\overline{U_i}$ and $\overline{\psi}$ as

$$\tilde{N} = Q_N * \overline{N} = Q_N * \left[D\frac{\partial \overline{\psi}}{\partial x_j}\frac{\partial \overline{\psi}}{\partial x_j} - \overline{(\tilde{U}_j - \overline{U_j})(\tilde{\psi} - \overline{\psi})}\frac{\partial \overline{\psi}}{\partial x_j} \right]. \tag{32}$$

Here, $\tilde{U}_i = Q_N * \overline{U_i}$ and $\tilde{\psi} = Q_N * \overline{\psi}$ are used to calculate N_{SS}. The resolved values $\tilde{\psi}$ and $\tilde{N}$ are calculated on the computational grid of LES and are interpolated on the particle positions. The interpolated values are used to calculate the mixing timescale according to Eq. (28). Other models for the scalar dissipation rate[36] can be used for the mixing volume model proposed in this study, and the improvement of the SGS scalar dissipation rate model will largely contribute to the accuracy of the LES–LP method.

2.3.3. Mixing volume model using two particles

The mixing volume model by Eq. (19) uses a large number of spatially separated particles in the mixing volume. Because molecular diffusion is the process which occurs in small scales,[1] the mixing model should act locally in the physical space by using small V_{M}^n. This means that particles close to each other are used in the mixing volume model. The requirement of low computational cost limits N_{P}, and then the number of particles close to one particle is also limited. Therefore, the localized mixing with small N_{P} requires that molecular diffusion is modeled by the interaction between a small number of particles. We consider the mixing volume model using two particles n and m for achieving the localized mixing. In this case, the mixing

volume is determined so that it contains only two particles. When $V_{\rm M}^n$ is set to involve the two particles n and m, the mixing volume model by Eq. (19) is represented by

$$\left[d\phi_\alpha^{(n)}/dt\right]_{\rm mix} = \frac{1}{\tau_{\rm M}}\left(\langle\phi_\alpha\rangle_{(n,m)} - \phi_\alpha^{(n)}\right), \tag{33}$$

$$\left[d\phi_\alpha^{(m)}/dt\right]_{\rm mix} = \frac{1}{\tau_{\rm M}}\left(\langle\phi_\alpha\rangle_{(n,m)} - \phi_\alpha^{(m)}\right). \tag{34}$$

Here, the average of ϕ_α in the mixing volume is given by $\langle\phi_\alpha\rangle_{(n,m)} = (\phi_\alpha^{(n)} + \phi_\alpha^{(m)})/2$, where $\langle*\rangle_{(n,m)}$ denotes an average of two particles n and m. In this case, the mixing timescale, Eq. (28), becomes

$$\tau_{\rm M} = \frac{\langle\psi''^2\rangle_{(n,m)}}{\langle N\rangle_{(n,m)}}, \tag{35}$$

where $\psi''^{(n)} = \psi^{(n)} - \langle\psi\rangle_{(n,m)}$ is the scalar fluctuation from $\langle\psi\rangle_{(n,m)}$. Eqs. (33) and (34) are the mixing volume model using two particles based on the IEM-type mixing scheme.

The conventional IEM-type mixing scheme using two particles is related to the Curl's model by the same mixing timescale.[37] Similarly, the mixing volume model using two particles can be also implemented in the form of the Curl's model.[38] In the mixing volume model based on the Curl's mixing scheme, the effect of molecular diffusion is modeled by following equations:

$$\left[d\phi_\alpha^{(n)}\right]_{\rm mix} = \beta\left[\langle\phi_\alpha\rangle_{(n,m)} - \phi_\alpha^{(n)}\right], \tag{36}$$

$$\left[d\phi_\alpha^{(m)}\right]_{\rm mix} = \beta\left[\langle\phi_\alpha\rangle_{(m,n)} - \phi_\alpha^{(m)}\right]. \tag{37}$$

Here, $[d\phi_\alpha^{(n)}]_{\rm mix}$ is the change in $\phi_\alpha^{(n)}$ during the time interval dt due to molecular diffusion, and $\beta = 1$ with probability $p_{\rm mix}$ and $\beta = 0$ with probability $(1-p_{\rm mix})$. The mixing probability $p_{\rm mix}$ is given by $p_{\rm mix} = 2dt/\tau_{\rm M}$,[39] where $\tau_{\rm M}$

is determined by Eq. (35). When the mixing occurs for particle n, Eqs. (36) and (37) are calculated for all of scalars $\mathbf{\Phi}^{(n)}$, and the scalar values of particles n and m are replaced by the averaged values in the mixing volume $\langle \phi_\alpha \rangle_{(n,m)}$. Both of the IEM model and Curl's model presented here are based on the interaction between two particles in the mixing volume. Although these models change the scalar variance according to the same mixing timescale τ_{M}, the difference in these mixing schemes has an influence on computed reactive scalar fields.[40,37]

In the mixing volume model using two particles, the mixing can be easily localized in the physical space by selecting the mixing partner m so that the distance between particles n and m is minimized in the physical space. Further localization in the scalar composition space $\mathbf{\Phi}$ might improve the mixing volume model when reactions occur mainly in an interfacial region of reactants.[1] In the mixing volume model, the localization in the physical and scalar composition spaces is related to the way to determine the mixing volume.

3. Application of the LES–LP method to a reactive planar jet

3.1. Reactive planar jet

The LES–LP method based on the ADM and the mixing volume model is tested for a planar jet with an isothermal chemical reaction A+B $\rightarrow$ P, which was previously investigated by using DNS.[27,41,28] The results of the LES–LP simulation are compared with the previous DNS data. Figure 2 shows a schematic of the reactive planar jet. Reactant A is supplied from the jet inlet of width d, and reactant B is supplied from the ambient flow. Product P is

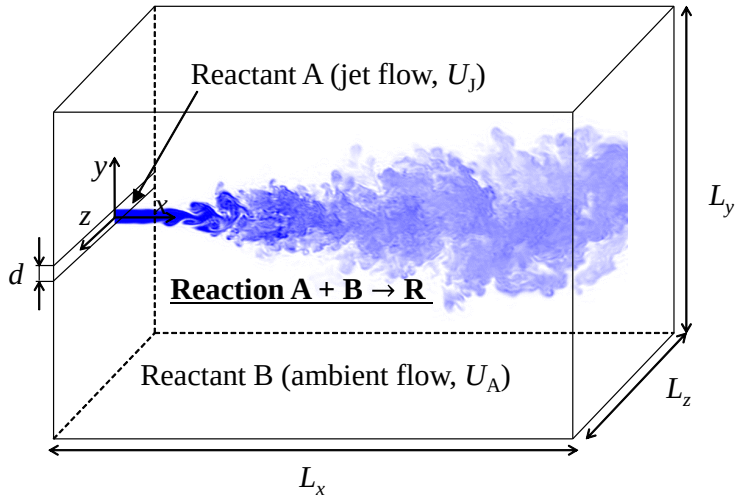

Figure 2: A planar jet with a second-order chemical reaction.

produced by the second-order chemical reaction A + B → P. The reactive species acts as a passive scalar. For simplicity, the molecular diffusivities of all reactive species are assumed to be equal ($D_\alpha = D$). The origin of the coordinate system is located at the center of the jet inlet. Streamwise, lateral, and spanwise directions are represented by x, y, and z, respectively. The Reynolds number $Re = U_J d/\nu$ is 2,200, and the Schmidt number of reactive species, $Sc = \nu/D$, is 1. Here, U_J is the mean bulk velocity at the jet inlet. The mean streamwise velocity of the ambient flow at $x = 0$ is $U_A = 0.056U_J$. The lateral profiles of mean velocity and rms value of the streamwise velocity fluctuation at the jet inlet were measured using the experimental apparatus.[42,43,44] These velocity statistics are used to determine the boundary condition at the jet inlet. Figure 3 shows the mean streamwise velocity $[U_{in}(y)]$ and the rms values of the velocity fluctuations $[u_{rms}(y)$, $v_{rms}(y)$, and

$w_{\rm rms}(y)]$ at the jet inlet. The measurement results of $U_{\rm in}(y)$ and $u_{\rm rms}(y)$ are also shown in Fig. 3. The lines in Fig. 3 are given by the following equations:

$$\frac{U_{\rm in}(y)-U_{\rm A}}{U_{\rm J}} = \sum_{n=0}^{5} A_n \left(\frac{y}{d}\right)^{2n}, \tag{38}$$

$$\frac{u_{\rm rms}(y)}{U_{\rm J}} = \sum_{n=0}^{5} B_{u,n} \left|\frac{y}{d}\right|^{n}, \tag{39}$$

$$\frac{v_{\rm rms}(y)}{U_{\rm J}} = \sum_{n=0}^{5} B_{v,n} \left|\frac{y}{d}\right|^{n}, \tag{40}$$

$$\frac{w_{\rm rms}(y)}{U_{\rm J}} = \sum_{n=0}^{5} B_{w,n} \left|\frac{y}{d}\right|^{n}. \tag{41}$$

The coefficients A_n, $B_{u,n}$, $B_{v,n}$, and $B_{w,n}$ are summarized in Table 1. The coefficients $B_{v,n}$ and $B_{w,n}$ are determined from the profiles of $v_{\rm rms}$ and $w_{\rm rms}$ in the turbulent channel flow,[45] although A_n and $B_{u,n}$ are determined from the experiment for the planar jet. The above equations are used to determine the boundary condition at the jet inlet.

The production rate of species α by the chemical reaction, S_α, is given by

$$S_{\rm P} = -S_{\rm A} = -S_{\rm B} = k\Gamma_{\rm A}\Gamma_{\rm B}, \tag{42}$$

where k is the reaction rate constant and Γ_α is the instantaneous concentration of species α. The initial concentration ratio of reactants A and B is set to $\Gamma_{\rm A0}/\Gamma_{\rm B0} = 2$. The mixture fraction ξ, which does not change with the chemical reaction, is defined to satisfy $\xi = 1$ at the jet inlet and $\xi = 0$ in the ambient flow:

$$\xi = \frac{\Gamma_{\rm A} - \Gamma_{\rm B} + \Gamma_{\rm B0}}{\Gamma_{\rm A0} + \Gamma_{\rm B0}}. \tag{43}$$

The stoichiometric value of the mixture fraction is $\xi_{\rm S} = \Gamma_{\rm B0}/(\Gamma_{\rm A0} + \Gamma_{\rm B0}) =$

Figure 3: Mean streamwise velocity and rms values of velocity fluctuations at jet inlet. Velocity statistics used for the boundary condition are compared with the measurement result.[42,43,44] u_{rms}: streamwise velocity. v_{rms}: cross-streamwise velocity. w_{rms}: spanwise velocity.

0.333. For the stoichiometric condition ($\xi = \xi_{\mathrm{S}}$), the maximum value of product concentration is $\mathit{\Gamma}_{\mathrm{P0}} = \mathit{\Gamma}_{\mathrm{A0}}\mathit{\Gamma}_{\mathrm{B0}}/(\mathit{\Gamma}_{\mathrm{A0}} + \mathit{\Gamma}_{\mathrm{B0}})$. The chemical production rate of product P normalized by U_{J}, d, and $\mathit{\Gamma}_{\mathrm{P0}}$ is given by $\hat{S}_{\mathrm{P}} = Da\hat{\mathit{\Gamma}}_{\mathrm{A}}\hat{\mathit{\Gamma}}_{\mathrm{B}}$, where $\hat{\mathit{\Gamma}}_{\alpha} = \mathit{\Gamma}_{\alpha}/\mathit{\Gamma}_{\alpha 0}$ and $Da = k(\mathit{\Gamma}_{\mathrm{A0}} + \mathit{\Gamma}_{\mathrm{B0}})d/U_{\mathrm{J}}$ is the Damköhler number. The numerical simulation is performed for the three chemical reactions, whose reaction rate constants satisfy $Da = 0.1$, 1, and 10. The Taylor microscale $\lambda_x = [\langle u^2\rangle/\langle(\partial u/\partial x)^2\rangle]^{1/2}$ is $0.25d$ at $(x, y) = (20d, 0)$, where u is the fluctuating component of the streamwise velocity U and $\langle * \rangle$ denotes the time-averaged value. The Kolmogorov scale $\eta = (\nu^3/\epsilon)^{1/4}$ is $0.015d$ at $(x, y) = (20d, 0)$.

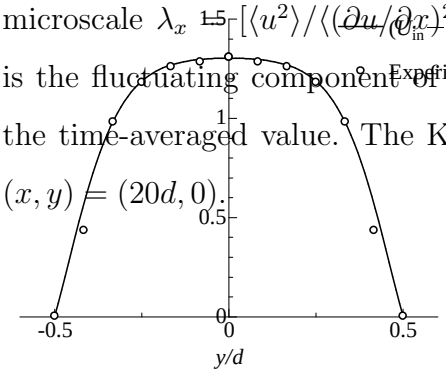

(a) Mean streamwise velocity

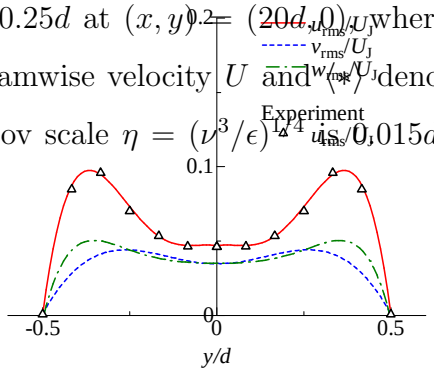

(b) Rms values of velocity fluctuations

Table 1: Coefficients in Eqs. (38) and (41) used to determine the boundary condition at the jet inlet.

n	0	1	2	3	4	5
A_n	1.303×10^{0}	-9.236×10^{-1}	-8.571×10^{0}	-1.207×10^{2}	3.464×10^{2}	0
$B_{u,n}$	4.673×10^{-2}	5.470×10^{-2}	-1.368×10^{0}	1.043×10^{1}	-1.657×10^{1}	0
$B_{v,n}$	3.505×10^{-2}	-1.558×10^{-2}	5.192×10^{-1}	-1.249×10^{0}	0	0
$B_{w,n}$	3.505×10^{-2}	-3.551×10^{-3}	1.930×10^{-1}	-1.186×10^{0}	7.355×10^{0}	-1.267×10^{1}

3.2. LES–LP simulation of a reactive planar jet

The LES–LP method is applied to the reactive planar jet explained above. The filtered velocity $\overline{U_i}$ and the filtered nonreactive scalar $\overline{\psi}$ are simulated by the LES based on the ADM. Here, similar to the mixture fraction, ψ is defined as $\psi = 1$ at the jet inlet and $\psi = 0$ in the ambient flow, and the molecular diffusivity for ψ is D. According to the reference DNS,[28] the LP method computes $\mathbf{\Phi} = (\xi, \mathit{\Gamma}_{\rm P})$, and the concentrations of reactants A and B are calculated by using the mass conservation law:[46]

$$\mathit{\Gamma}_{\rm A} = \mathit{\Gamma}_{\rm A0}\xi - \mathit{\Gamma}_{\rm P}, \tag{44}$$

$$\mathit{\Gamma}_{\rm B} = \mathit{\Gamma}_{\rm B0}(1-\xi) - \mathit{\Gamma}_{\rm P}. \tag{45}$$

The size of the computational domain is $L_x \times L_y \times L_z = 9.5\pi d \times 7.7\pi d \times 2.6\pi d$.

The numerical method and computational parameters of the LES and the LP method are shown in Sec. 3.3 and Sec. 3.4, respectively. The reference DNS was conducted using the numerical scheme similar to the present LES, and the detail of the numerical method can be seen in previous papers.[41,28] In these papers, it was also shown that the mean flow and scalar

developments and the self-similar profiles of rms velocity agree well with the experiments[42,43,44] used for determining the inflow boundary conditions. The number of the computational grid point in the DNS was $N_x \times N_y \times N_z = 700 \times 430 \times 74$ in the streamwise, lateral, and spanwise detections.

3.3. Numerical method and computational parameters of LES

The present LES is based on the same numerical method as in the reference DNS.[41,28] A finite-difference method is used in the LES. The fully conservative fourth-order central difference scheme[47] is used for spatial discretization in the x and z directions, and the fully conservative second-order central difference scheme[47] is used in the y direction. The continuity equation and the Navier–Stokes equations are solved by using the fractional step method. The Poisson equation is solved by the conjugate gradient method. The hybrid implicit/explicit scheme[48] is used for the time integration, where the Crank–Nicolson method is used for the viscous and molecular diffusion terms in the y direction and the third-order Runge–Kutta method is used for the other terms. The explicit filter with a five-point stencil proposed by Stolz et al.[14] is used as the low-pass filter G. We set $N_{\mathrm{D}} = 5$ in Eq. (10) to obtain Q_N. The LES based on the ADM is performed by the method using the explicit filter instead of the relaxation term proposed by Mathew et al.[30] Thus, the composite filter $(Q_N * G)$, which removes the small-scale fluctuations, is applied to the velocity and the passive scalar every three time steps instead of adding the relaxation terms.

The convective boundary condition[49] is applied to the outlet boundary (the y–z plane at $x = L_x$). At the lateral boundaries, the y-directional gradient of velocity is set to 0, and the periodic boundary condition is applied

for the spanwise direction. The inflow velocity at $x = 0$ is generated by superimposing random fluctuations onto the mean velocity. At the jet inlet, the inflow velocity is generated according to Eqs. (38) and (41). In the ambient flow, the inflow velocity is set to U_{A} without any fluctuations. For the scalar, $\psi = 1$ and 0 are imposed at the jet inlet and in the ambient flows, respectively, except for the outlet boundary, at which the convective boundary condition is applied. Here, similar to the convective boundary condition for the velocity,[49] the y and z directional molecular diffusion terms are added to the conventional convective boundary condition for ψ.

The LES–LP method is applied for two different computational grid of LES. $N_x \times N_y \times N_z = 300 \times 214 \times 50$ grid points are used in the fine-grid LES, whereas $N_x \times N_y \times N_z = 190 \times 190 \times 32$ grid points are used in the coarse-grid LES. The results for these two grids are compared for investigating how the unresolved scales affect the numerical results. In the y direction, a fine grid is used near the jet centerline, and the grid is stretched near the lateral boundaries. The sizes of the computational grids $(\Delta x, \Delta y, \Delta z)$ are $(0.099d, 0.054d, 0.16d) = (0.40\lambda_x, 0.22\lambda_x, 0.64\lambda_x)$ and $(0.16d, 0.061d, 0.26d) = (0.64\lambda_x, 0.24\lambda_x, 1.04\lambda_x)$ for the fine-grid and coarse-grid LES, respectively, where λ_x at $(x, y) = (20d, 0)$ is used for evaluating the grid size. da Silva et al.[50] compared the LES and DNS of planar jets with a passive scalar, and showed that LES of planar jets requires the grid size smaller than one Taylor microscale λ for capturing the large-scale characteristics of planar jets. In their simulations, $\lambda = 0.16d$. From their criteria on the resolution, we find that the grid sized in the fine-grid LES is small enough to capture the large-scale characteristics. The coarse-grid LES has a

Table 2: Computational parameters for the LES–LP simulations.

	N_{P}	ρ_{P}	δ_{P}	$(N_x \times N_y \times N_z)/N_{\mathrm{P}}$
Coarse-grid LES	$10,000$	$1.70d^{-3}$	$0.520d$	115.5
	$30,000$	$5.09d^{-3}$	$0.361d$	38.5
	$60,000$	$10.2d^{-3}$	$0.286d$	19.3
Fine-grid LES	$60,000$	$10.2d^{-3}$	$0.286d$	53.5

resolution close to the limitation shown by da Silva et al.[50] The time step is set to $dt = 0.02d/U_{\mathrm{J}}$ for all simulations. The maximum CFL number $dtU/\Delta x$ at the jet inlet is 0.28 for the fine grid LES and 0.18 for the coarse grid LES.

3.4. Numerical method and computational parameter of LP method

The variables computed by the LES are spatially interpolated at the particle positions by using a tri-linear interpolation. Equation (18) is solved by using the fractional step method:[6]

$$\phi_{\alpha\mathrm{M}}^{(n)}(t) = \phi_{\alpha}^{(n)}(t) + \left[d\phi_{\alpha}^{(n)}\right]_{\mathrm{mix}}, \tag{46}$$

$$\phi_{\alpha}^{(n)}(t+dt) = \phi_{\alpha\mathrm{M}}^{(n)}(t) + S_{\alpha}(\mathbf{\Phi}_{\mathrm{M}}^{(n)})dt. \tag{47}$$

Here, the subscript M indicates that the effect of molecular diffusion has been computed for the quantity. Molecular diffusion is modeled by the mixing volume model using two particles implemented by the IEM-type mixing scheme [Eqs. (33) and (34)] or Curl's mixing scheme [Eqs. (36) and (37)]. The results are compared between the two mixing schemes. In the IEM model, $[d\phi_{\alpha}^{(n)}]_{\mathrm{mix}}$ is computed as $[d\phi_{\alpha}^{(n)}/dt]_{\mathrm{mix}}dt$. When dt/τ_{M} is larger than 1 in the IEM model, $\phi_{\alpha}^{(n)}$ and $\phi_{\alpha}^{(m)}$ are replaced by $\langle\phi_{\alpha}\rangle_{(n,m)}$ instead of using Eqs. (33)

and (34). This can happen when the two particles are located very close to each other even if the computational time step dt is small compared with the minimum timescale of the scalar filed. In the mixing volume model using two particles, the nearest particle is selected as a mixing partner.

The number of particles $N_{\rm P}$ determines the spatial resolution of the LP simulation. The LP simulation is conducted for $N_{\rm P} = 60,000$ with the fine-grid LES using the Curl's model. For the coarse-grid LES, the LP method is applied for $N_{\rm P} = 10,000$, $30,000$, and $60,000$ for investigating the dependence of the LP method on $N_{\rm P}$. The coarse grid LES–LP simulations are used for the comparison between the IEM-type mixing scheme and Curl's mixing scheme. Table 2 shows the number density of particles, $\rho_{\rm P} = N_{\rm P}/(L_x \times L_y \times L_z)$, the mean distance between the nearest particles, $\delta_{\rm P} = (4\pi\rho_{\rm P}/3)^{-1/3}$, and the grid number used in the LES occupied by one particle, $(N_x \times N_y \times N_z)/N_{\rm P}$, for each simulation. It is found that $N_{\rm P}$ is less than the number of LES grid points $(N_x \times N_y \times N_z)$, and $\delta_{\rm P}$ is slightly larger than the Taylor microscale λ_x.

Initially, the particles are randomly distributed in the computational domain. From a statistical point of view, the number density of particles is constant and is homogeneous in the entire computational domain because of the incompressible condition. A periodic boundary condition is applied to the z direction for the particles. The y–z plane at $x = 0$ and the lateral boundaries are set to the inflow boundary, whereas the y–z plane at $x = L_x$ is set to the outflow boundary. A particle that leaves the computational domain across the inflow or outflow boundary is replaced on the inflow boundary. To keep the local number density of particles statistically constant, the position

where the particle is replaced is determined according to the local flow rate across the inflow boundary.[1] In the LES, the instantaneous local flow rate normal to the inflow boundary is calculated for the computational grids on the boundary. The computational grid at which the particle is replaced is determined so that the number of replaced particles is proportional to the local flow rate toward the computational domain. After the grid at which the particle is replaced is determined, the particle is randomly placed on the grid. When the particle is replaced at the inflow boundary, $\xi^{(n)} = 1$ and $\mathit{\Gamma}_{\mathrm{P}}^{(n)} = 0$ are imposed for the particle at the jet inlet, and $\xi^{(n)} = 0$ and $\mathit{\Gamma}_{\mathrm{P}}^{(n)} = 0$ are imposed for the particle in the ambient flow.

The mixing volume model using two particles is implemented by the procedure below. In the simulation, all particles are numbered to identify them. Because the particles are randomly distributed in the computational domain, the number assigned to the particles is independent of the location of particles. The mixing is calculated for particles in number order. All particles have a mixing partner, and the particles after mixing are not eliminated from the candidate as a partner for mixing of other particles. In this mixing scheme, one particle can participate more than one mixing events per one time step. The mixing timescale is calculated at each time step for each pair.

Statistics are estimated from the particle fields. The computational domain is divided into 80×100 grid cells in the x and y directions. Statistics are calculated in each cell by taking the cloud-in-cell ensemble average[1] (i.e., the ensemble average of particles located in the cell). Because this grid cell has a spanwise length of L_z, the statistics are averaged in the z direction. The statistics are calculated by taking time-average over [time] steps, which is [tt]

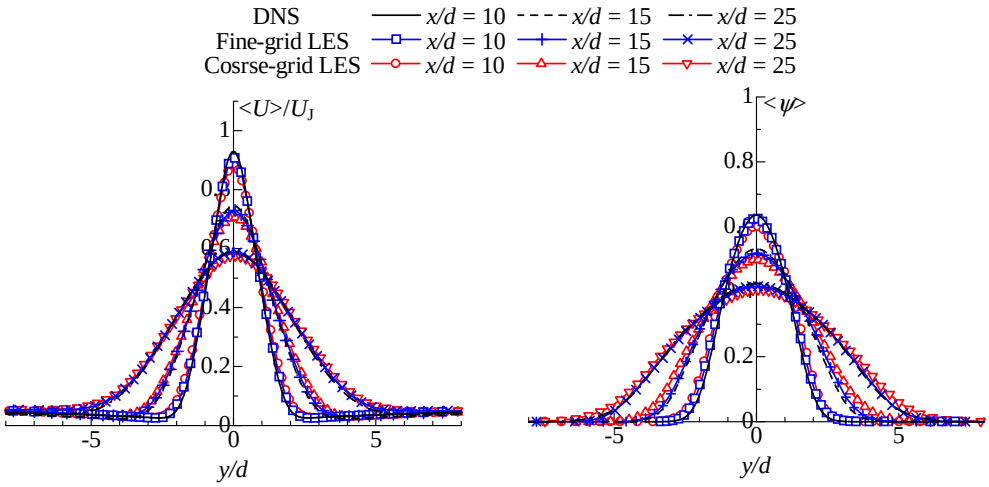

(a) Mean streamwise velocity (b) Mean nonreactive scalar

Figure 4: Cross-streamwise profiles of mean streamwise velocity and mean scalar obtained by LES and DNS.

times longer than the flow time unit defined by $2L_x/(U_\mathrm{J} + U_\mathrm{A})$. The statistics are calculated after a time $t = 2,400d/U_\mathrm{J}$. It should be noted that these 80×100 cells are only used to calculate the statistics and are independent of the evolutions of particles in the physical and composition spaces. It was confirmed that a smaller cell (140×200) yields similar profiles of statistics presented in this paper.

4. Results and discussion

4.1. LES results

The LES results are compared with the DNS results. In the LES, the time-averaged statistics are estimated from the unfiltered quantities. Figure 4 shows the mean streamwise velocity ($\langle U \rangle$) and mean scalar ($\langle \psi \rangle$). Figure 5

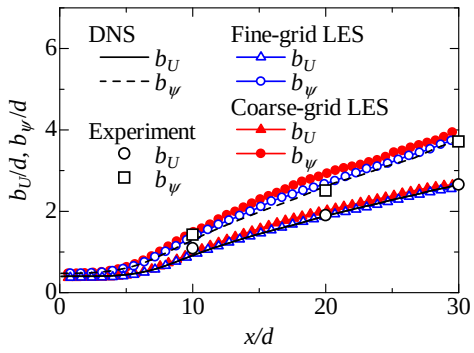

Figure 5: Jet half-widths based on mean streamwise velocity (b_U) and mean scalar (b_ψ). The LES results are compared with the DNS[41,28] and experiments[43,44] of planar jets with the similar Reynolds numver. In the experiments, b_ψ is obrained from the concentraion measurements of a diffusive dye, whose Schmidt number is $Sc = 600$, although $Sc = 1$ in the LES and DNS.

compares the jet half-widths (b_U and b_ψ) based on $\langle U \rangle - U_\mathrm{A}$ and $\langle \psi \rangle$ among the LES, DNS,[41,28] and experiments[43,44] of planar jets. Although the Schmidt number is much larger than 1 in the experiments ($Sc = 600$), we use the experimental results for comparison because the molecular diffusion has only a neglegible influence on the mean scalar field for Sc which is not much smaller than 1.[51] For both fine and coarse grids, the LES based on the ADM predicts well the profiles of $\langle U \rangle$ and $\langle \psi \rangle$. The jet half-width obtained in the LES is also similar to the DNS and experiments, and increases in proportion to x in the self-similar regions. However, b_ψ is slightly overpredicted by the LES. This tendency can be also found in the LES results by da Silva et al.[50] They also showed that when the grid size is larger than $\lambda \approx 0.16d$, the LES provides the jet spreading rate much larger than the DNS for the mean scalar fields.

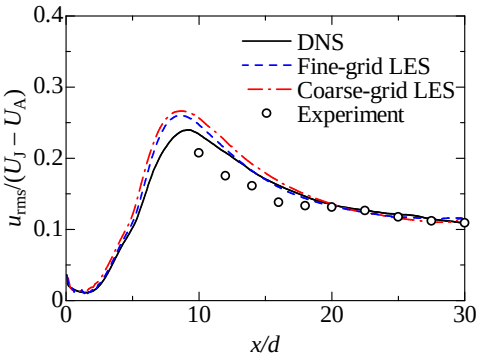

Figure 6: Streamwise evolution of streamwise rms velocity $u_{\rm rms}$ on the jet centerline. The LES results are compared with the DNS[41,28] and experiments[43,44] of planar jets with the same Reynolds numver.

Figure 6 shows the streamwise rms velocity on the jet centerline. Although the inflow velocity is generated so that the rms velocity sarisfies Eq. (41), a large part of velocity fluctuationsdecays at the jet inlet. However, after the initial deday, there still exist velocity fluctuations, which promote the development of planar jets. Although the LES results are similar to the DNS and experiment especially in the downstream region, the peak value in $u_{\rm rms}$ is overpredicted by the LES. The development of the mean velocity and scalar fields strongly depends on the inflow velocity.[52] The inflow velocity generated by random fluctuations is different from real turbulence. However, the agreement in the jet half-width between the numerical simulations and the experiments justifies the application of the random fluctuations as the inflow velocity for the planar jet investigated in this study.

Figure 7 shows the cross-streamwise profiles of the rms values of the streamwise velocity and scalar fluctuations ($u_{\rm rms}$ and $\psi_{\rm rms}$). The rms values

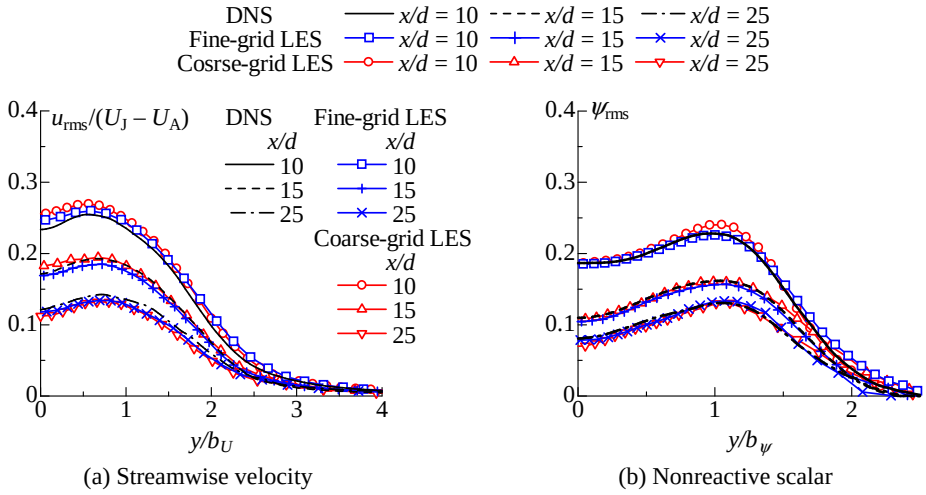

Figure 7: Cross-streamwise profiles of rms values of streamwise velocity and nonreactive scalar fluctuations obtained by LES and DNS. The cross-streamwise coordinate y is normalized by the half-widths (b_U and b_ψ).

obtained by the LES are close to the DNS data. Thus, good agreement with the DNS data is achieved for the mean and rms values by the LES based on the ADM for both fine and coarse grids.

4.2. Instantaneous scalar fields represented by particles

The same boundary condition is used for ψ in the LES and ξ in the LP simulation. Therefore, these two scalars should have similar instantaneous profiles in the LES–LP simulation. Figure 8 compares ψ on the x–y plane at $z = 0$ with ξ represented by the particles located near $z = 0$ ($|z/d| < 0.5$). The mixture fraction is diffused in the y direction with the jet development. In the large-scale distribution, ξ is similar to ψ. The spatial resolution of the LP method is related to the distance between particles. Because δ_P is

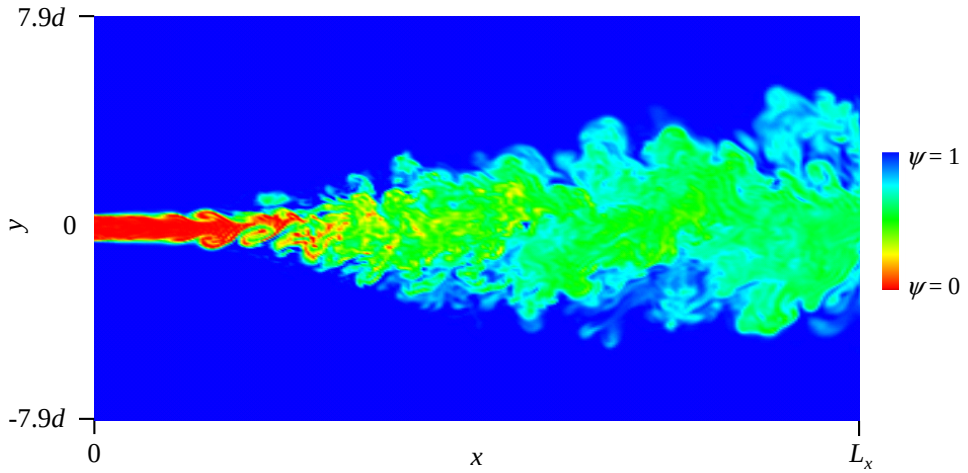

(a) Instantaneous scalar field (LES)

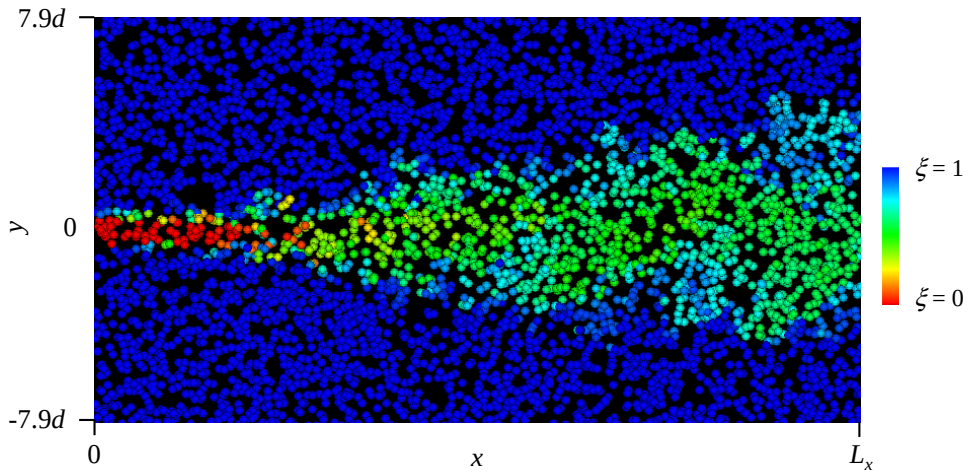

(b) Instantaneous mixture fraction (Particle field)

Figure 8: Instantaneous nonreactive scalar profiles. The results obtained by the fine-grid LES–LP simulation using $60,000$ particles are visualized. (a) ψ computed by the fine-grid LES (x–y plane at $z = 0$). (b) Mixture fraction ξ computed by the LP method. The particles in the region $|z/d| < 0.5$ are visualized. The color of particles shows a value of $\xi^{(n)}$.

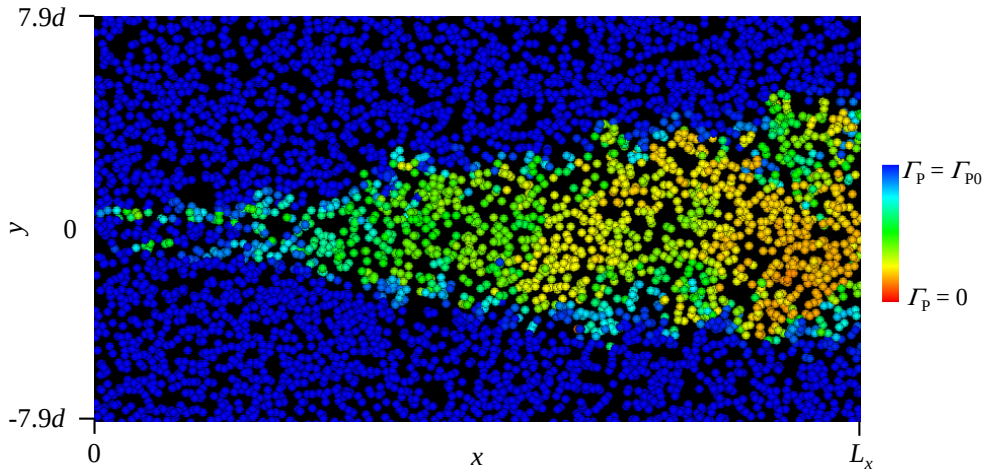

Figure 9: Instantaneous concentration of product P for $Da = 1$ represented by particles near $z = 0$ ($|z/d| < 0.5$). The color of particles shows a value of $\Gamma_P^{(n)}$. The results obtained by the fine-grid LES–LP simulation using $60,000$ particles are visualized.

not small, the small-scale scalar field cannot be represented by the particles. Near the jet inlet, the spanwise vorticities appear in the shear layer, and their existence is observed in the profile of ψ [Fig. 8(a)]. However, the pattern which is related to the spanwise vortical structure does not appear in ξ [Fig. 8(b)] because the distance between the particles is not small enough to resolve this structure.

Figure 9 shows Γ_P represented by the particle field. Because of the progress of the reaction, Γ_P increases in the downstream direction. Near the jet inlet, product P exists only in the interfacial region between the jet and ambient flows. Thus, the reaction starts in this interfacial region. Then, the chemical product spreads with the jet development. Similar profiles of Γ_P are observed in the reference DNS.[28]

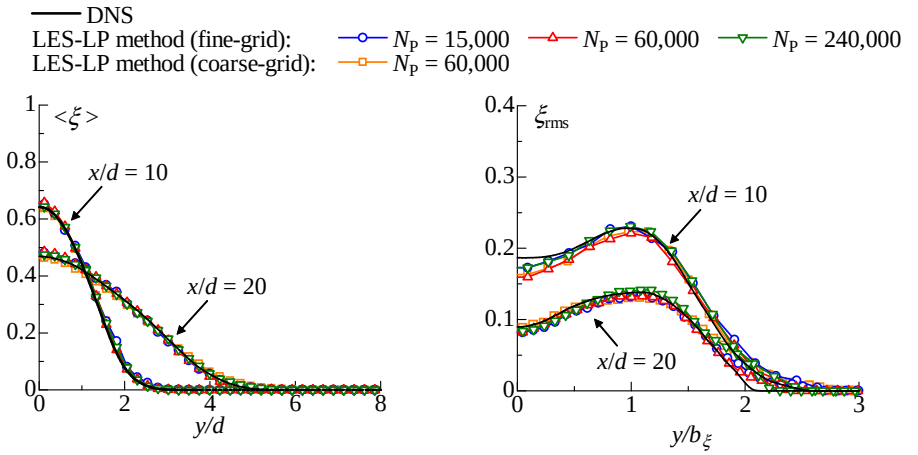

(a) Mean mixture fraction (b) Rms value of mixture fraction fluctuation

Figure 10: Cross-streamwise profiles of (a) mean mixture fraction and (b) rms value of mixture fraction fluctuation at $x/d = 10$ and 20 obtained by DNS and LES–LP simulation. In Fig. (b), the jet half-width b_ξ based on $\langle\xi\rangle$ is used to normalize y.

4.3. Nonreactive scalar statistics computed from particle field

In the LP method, the nonreactive scalar value of each particle changes only by the mixing model as shown in Eq. (18). Therefore, the statistics of ξ can be used for validating the mixing model and the model for the mixing timescale. Because the mixing timescale changes depending on the distance between the mixing particles, the statistics of ξ obtained from the particles are compared between the DNS result and the fine-grid LES–LP simulations with different N_P for investigating the validity of the model for the mixing timescale. The LES–LP simulations based on the fine-grid and coarse-grid LESs are compared for investigating the effect of the unresolved velocity and scalar fields.

Figures 10(a) and (b) show the mean mixture fraction $\langle\xi\rangle$ and the rms

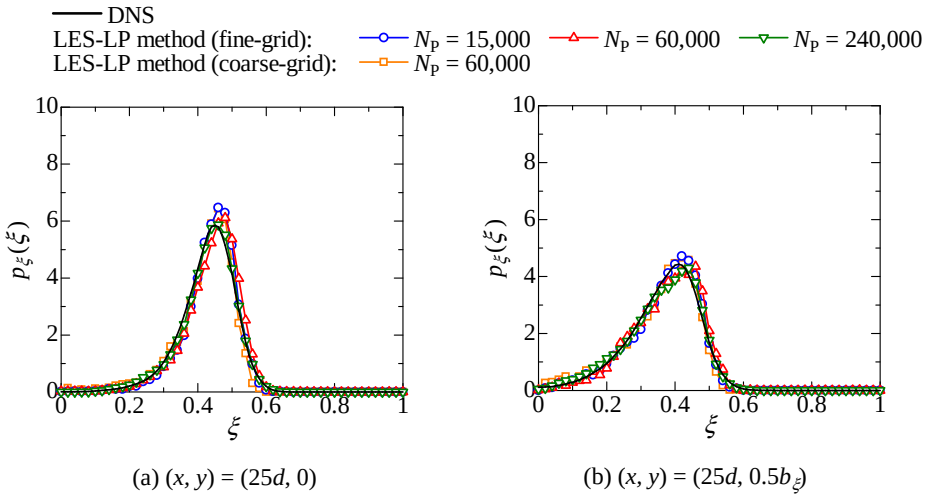

Figure 11: Probability density function of mixture fraction at (a) $(x, y) = (25d, 0)$ and (b) $(x, y) = (25d, 0.5b_\xi)$ obtained by DNS and LES–LP simulation.

values of the mixture fraction fluctuation $\xi_{\rm rms}$. In Fig. 10(b), the jet half-width b_ξ based on $\langle\xi\rangle$ is used to normalize y. The profile of $\langle\xi\rangle$ is hardly affected by the molecular diffusion term because the mean molecular diffusion term is often negligible in the mean scalar transport equation.[6] Therefore, Eqs. (17) and (18) show that $\langle\xi\rangle$ is mainly determined by the resolved velocity field in the LES–LP simulation. In Fig. 10(a), $\langle\xi\rangle$ shows good agreement between the DNS and the LES–LP simulations, and is independent of $N_{\rm P}$ and the size of the LES grid. In the DNS, all scales of velocity fields are taken into account in the mean scalar profile. This agreement and the independence on the grid size indicate that the unresolved velocity hardly affects the mean nonreactive scalar profile. In Fig. 10(b), $\xi_{\rm rms}$ obtained by the particle field also agrees well with the DNS results. As shown in the derivation of the model

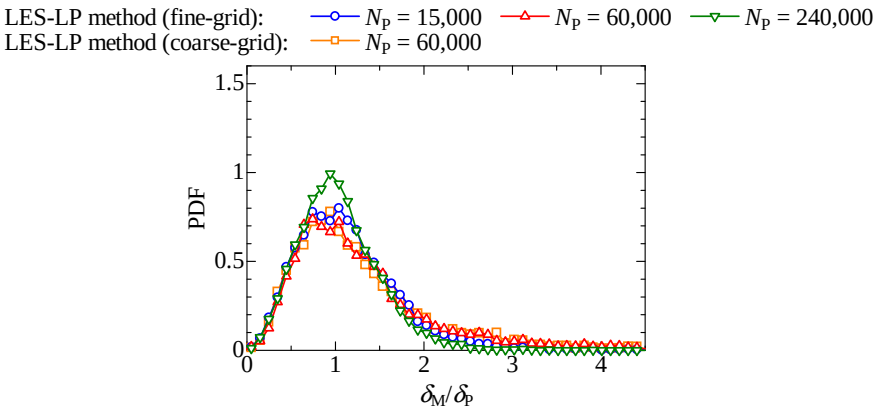

Figure 12: Probability density function of distance between mixing particles δ_{M} at $(x, y) = (20d, 0)$. The distance δ_{M} is normalized by the mean distance between the nearest particles δ_{P}.

for τ_{M}, the decay of scalar fluctuations strongly depends on τ_{M}. Therefore, the agreement in ξ_{rms} shows that τ_{M} is properly determined by the method described in the previous section. It is also found that the number of particles and the grid size in the LES have a very small influence on ξ_{rms} in the LES–LP simulation. Figure 11 shows the probability density function (PDF) of ξ. The PDF obtained by the LES–LP method is similar to the DNS result. In the LES–LP simulation, the mixture fraction of particles is imposed to satisfy $\xi^{(n)} = 0$ or 1 at the inflow boundary. A value of $0 < \xi^{(n)} < 1$ is caused by molecular diffusion modeled by the mixing model. Thus, the agreement in the PDF for $0 < \xi^{(n)} < 1$ also shows the validity of the mixing model.

Figure 12 shows the PDF of the distance between the mixing pair in the two particle mixing model (δ_{M}) normalized by δ_{P}. The nearest particle is selected as a mixing partner in the simulation. However, because the

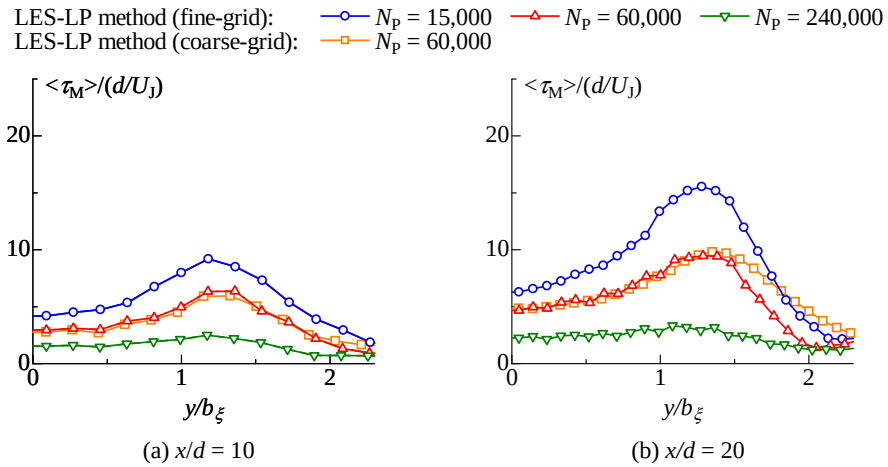

Figure 13: Cross-streamwise profiles of mean mixing timescale.

particles are randomly distributed in the physical space, δ_M can be larger or smaller than δ_P. The PDF has a large value for $\delta_M/\delta_P \approx 1$, and the length scale which characterizes the mixing event is δ_P. Figure 13 shows the mean mixing timescale $\langle\tau_M\rangle$. The mixing timescale depends on the location in the flow field. Comparing $\langle\tau_M\rangle$ between the fine and coarse grids, one can see that $\langle\tau_M\rangle$ is independent of the grid size except for the edge of the jet at $x/d = 20$. Thus, the unresolved part of ψ has a small influence on the mixing timescale determined by Eq. (35). For different N_P, molecular diffusion is modeled by the mixing model at different length scales because δ_P changes with N_P. Therefore, τ_M strongly depends on N_P, and as N_P increases $\langle\tau_M\rangle$ decreases. In the LES–LP simulations, ξ_{rms} is almost independent of N_P, and its streamwise decay in the LP simulation is similar to the DNS result. Thus, τ_M is controlled by the present model so that the decay of the scalar fluctuation obeys the scalar dissipation rate estimated from the LES. These

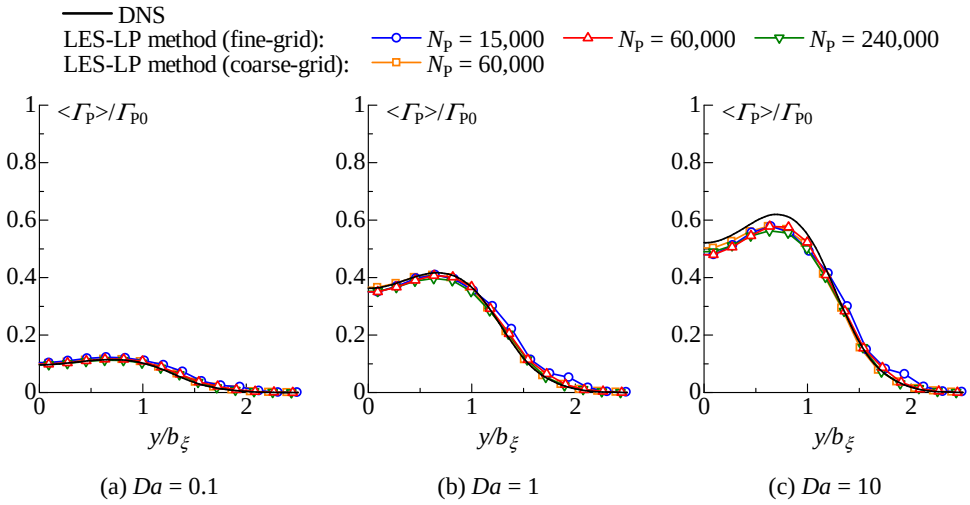

Figure 14: Cross-streamwise profiles of mean concentration of product P at $x/d = 10$. (a) $Da = 0.1$. (b) $Da = 1$. (c) $Da = 10$.

results show that the length scale effect on the mixing model is taken into account in τ_M. It should be noted that the control of τ_M is done without adjusting any model parameters.

4.4. Statistics of concentrations of reactive species

Figures 14 and 15 compare the mean concentration of product P, $\langle \Gamma_P \rangle$, between the LES–LP simulation and the DNS. As Da increases, $\langle \Gamma_P \rangle$ becomes large. At $x/d = 10$, the cross-streamwise profiles of $\langle \Gamma_P \rangle$ have a peak value away from the jet centerline for $Da = 1$ and 10. However, $\langle \Gamma_P \rangle$ is almost independent of the cross-streamwise location near the jet centerline at $x/d = 25$. At $x/d = 10$, $\langle \Gamma_P \rangle$ for $Da = 10$ in the LES–LP simulations is slightly small compared with the DNS result. When the Damköhler number is large, the chemical reaction rate is controlled by the mixing process because the

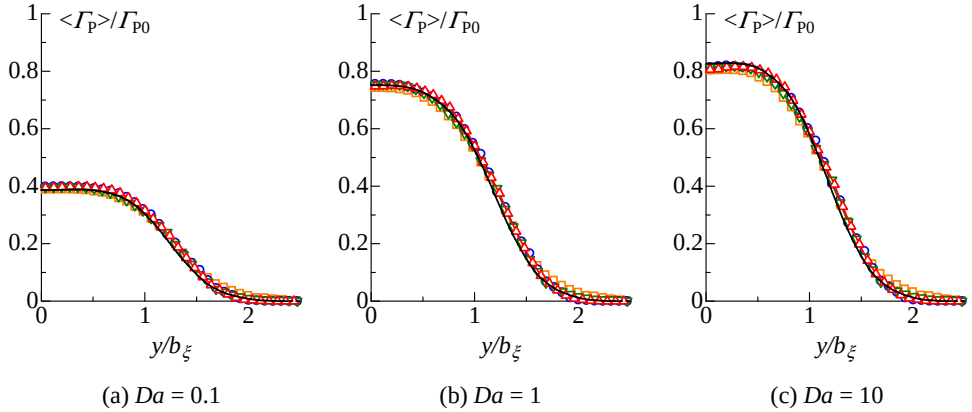

Figure 15: Cross-streamwise profiles of mean concentration of product P at $x/d = 25$. (a) $Da = 0.1$. (b) $Da = 1$. (c) $Da = 10$. Symbols and lines are the same as in Fig. 14.

chemical reaction proceeds extremely fast after the two reactants are mixed by molecular diffusion. Therefore, the choice of the mixing model could affect the statistics of reactive scalars for fast chemical reactions. Although there is a small discrepancy in $\langle \Gamma_{\rm P} \rangle$ for $Da = 10$, the profiles of $\langle \Gamma_{\rm P} \rangle$ obtained by the LES–LP method agree well with the DNS results, and are independent of $N_{\rm P}$ and the size of the LES grid. Figure 16 shows the mean concentration of A, $\langle \Gamma_{\rm A} \rangle$. Equation (44) shows that $\langle \Gamma_{\rm A} \rangle$ is determined by $\langle \xi \rangle$ and $\langle \Gamma_{\rm P} \rangle$, whose profiles are shown in detail above. Therefore, only the results of the fine-grid LES–LP simulation using $60,000$ particles are compared with the DNS results. The concentration of A in the nonreactive flow is obtained by $\Gamma_{\rm A} = \Gamma_{\rm A0}\xi$, which is derived by substituting $\Gamma_{\rm P} = 0$ into Eq. (44). It is found that $\langle \Gamma_{\rm A} \rangle$ is decreased by the reaction, and its profile is quite similar between the LES–LP simulation and the DNS. Thus, the mean concentration profiles of reactive species are well predicted by the LES–LP method.

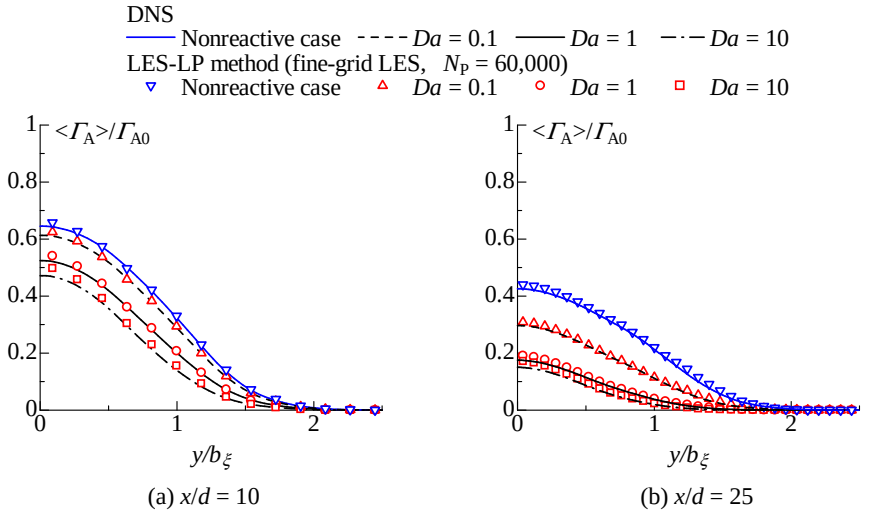

Figure 16: Cross-streamwise profiles of mean concentration of reactant A. The results of the fine-grid LES–LP simulation using $N_{\mathrm{P}} = 60,000$ particles are compared with the DNS results.

Figure 17 shows the cross-streamwise profile of the mean normalized chemical production rate of P, $\langle \hat{S}_{\mathrm{P}} \rangle$, at $x/d = 10$. For $Da = 10$, $\langle \hat{S}_{\mathrm{P}} \rangle$ is large away from the jet centerline. This is because the fast reaction takes place in the interfacial region between the jet and ambient fluids. The large production rate away from the jet centerline is related to large $\langle \Gamma_{\mathrm{P}} \rangle$ in this region [Fig. 14(c)]. For $Da = 0.1$ and 1, $\langle \hat{S}_{\mathrm{P}} \rangle$ is almost independent of the cross-streamwise location near the jet centerline. The results of the LES–LP simulation is similar to the DNS results. However, $\langle \hat{S}_{\mathrm{P}} \rangle$ for $Da = 10$ slightly depends on the computational parameters in the LES–LP method. The fast reaction strongly depends on the mixing process, which is modeled in the LES–LP method. Therefore, the reaction rate in this method can depend on N_{P}, which determines the scale at which molecular diffusion

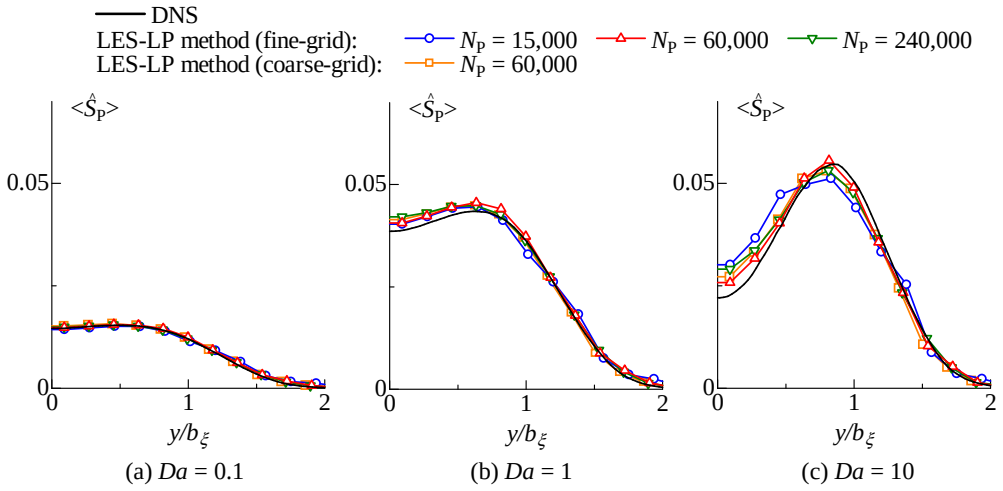

Figure 17: Cross-streamwise profiles of mean normalized chemical production rate of product P at $x/d = 10$. (a) $Da = 0.1$. (b) $Da = 1$. (c) $Da = 10$.

is modeled. However, for all of the LES–LP simulations, the discrepancy from the DNS results is small, and the reaction rate is well predicted by the LES–LP method.

Figure 18 shows the PDF between Γ_A and Γ_P at $(x, y) = (25d, 0)$. It is found that the reaction decreases and increases Γ_A and Γ_P, respectively. For $Da = 10$, the PDF of Γ_A has a nonzero value even for $\Gamma_A = 0$ because the reaction consumes most of reactant A. The PDF of Γ_P has a large peak for $Da = 0.1$, and its distribution spreads as Da increases. The LES–LP method captures well these changes in the PDF due to the reaction. Figure 19 shows the joint PDF of Γ_A and Γ_B for $Da = 1$ at $(x, y) = (15, 0)$. In the nonreactive flow, the concentrations of A and B are related to each other by $\Gamma_B/\Gamma_{B0} = 1 - \Gamma_A/\Gamma_{A0}$. Because Γ_A and Γ_B decrease with the reaction, the joint PDF of Γ_A and Γ_B maps in the region away from the line $\Gamma_B/\Gamma_{B0} = 1 - \Gamma_A/\Gamma_{A0}$. The

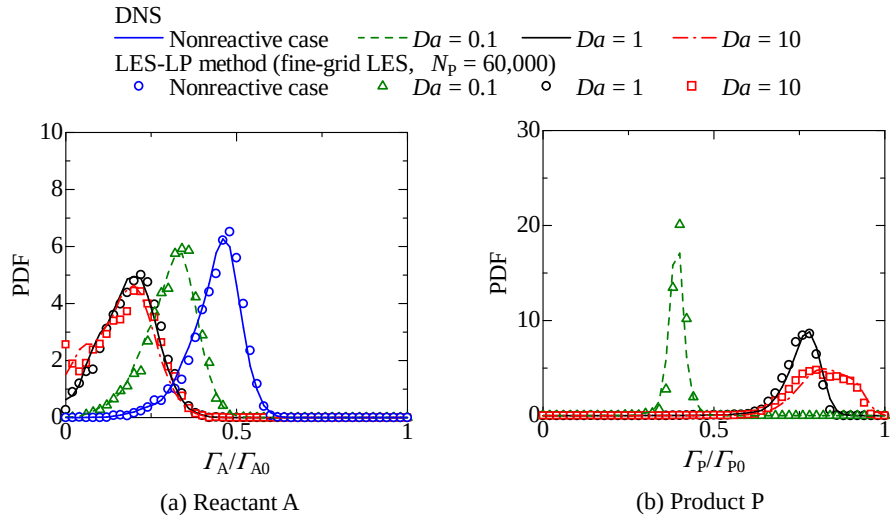

(a) Reactant A (b) Product P

Figure 18: Probability density function of concentration of (a) reactant A and (b) product P at $(x, y) = (25d, 0)$. The results of the fine-grid LES–LP simulation using $N_{\mathrm{P}} = 60,000$ particles are compared with the DNS results.

profile of the joint PDF is very similar between the DNS and the LES–LP simulation. Thus, the relationship between the concentrations of the two reactants, which determines the reaction rate by $k\Gamma_{\mathrm{A}}\Gamma_{\mathrm{B}}$, is well captured by the LES–LP method.

5. Concluding remarks

A numerical method for turbulent reactive flows was developed by combining the LES based on the ADM with the Lagrangian particle method (LES–LP method). In this approach, the LES computes the filtered velocity and the filtered nonreactive scalar using the ADM. The reactive scalars are computed by using the Lagrangian notional particles for precluding the

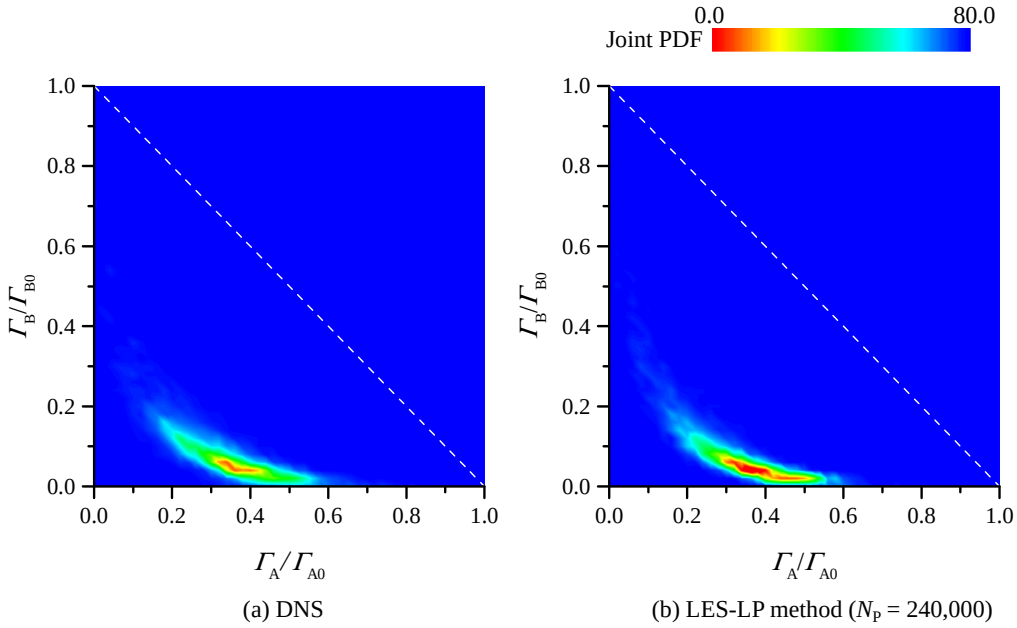

Figure 19: Joint probability density function between concentrations of reactants A and B for $Da = 1$ at $(x, y) = (15d, 0)$. (a) DNS. (b) Fine-grid LES–LP simulation using $N_{\mathrm{P}} = 240,000$ particles. The concentrations for the nonreactive case, $\Gamma_{\mathrm{B}}/\Gamma_{\mathrm{B0}} = 1 - \Gamma_{\mathrm{A}}/\Gamma_{\mathrm{A0}}$, is shown by a white broken line.

problems on modeling of chemical source terms. Values of reactive scalars are assigned to each particle. The evolutions of Lagrangian particles in physical and scalar composition spaces are modeled by using the resolved velocity fields and the mixing model. We proposed the mixing model based on the mixing volume concept, in which the mixing timescale of the model is determined by relating the decay of scalar variance to the dissipation in the mixing volume. In the LES–LP method, the mixing timescale is estimated from the filtered nonreactive scalar field computed by the LES. The present mixing

model and mixing timescale model do not have any model parameters.

The LES–LP method was applied to a planar jet with a second-order chemical reaction $A + B \rightarrow P$ to demonstrate its performance. The LES based on the ADM captures well the large-scale velocity and scalar fields, and the statistics in the LES show good agreement with the DNS data. The results show that the mixture fraction statistics obtained from the particles also agree well with the DNS data, and hardly depend on the computational parameters (the size of the LES grid and the number of particles). This agreement shows that the evolution of nonreactive scalar is well modeled in the LES–LP simulation by using the resolved velocity and the present mixing model. The independence on the number of particles means that the mixing timescale is well adjusted so that the scalar variance decays according to the scalar dissipation rate estimated from the LES. The statistics of concentrations of reactive species (mean concentration, mean reaction rate, and PDFs) in the LES–LP simulation were compared with the previous DNS results. For a fast reaction, the mean concentration of product P is slightly underpredicted by the LES–LP method. As a whole, the statistics obtained by the LES–LP method were shown to be in good agreement with the DNS data. These results showed that the LES–LP method based on the ADM and the mixing model can be useful for predicting turbulent reactive flows.

Acknowledgment

The authors would like to thank Dr. Takashi Kubo for his valuable comments on this study. Part of the work was carried out under the Collaborative Research Project of the Institute of Fluid Science, Tohoku University. This work was supported by JSPS KAKENHI Grant Number 25002531 and

MEXT KAKENHI Grant Numbers 25289030, 25289031, and 25630052.

Appendix A. Nomenclature

d	inlet width of planar jet
D	diffusivity coefficient of passive scalar
Da	Damköhler number
G	filtering operator
k	reaction rate constant
N	scalar disspation rate of ψ or ϕ_α with subscript α
N_P	number of particles used in simulation
Re	Reynolds number
Sc	Schmidt number
S_α	chemical source term for ϕ_α or Γ_α
t	time
$\mathbf{U} = (U, V, W)$	velocity
U_J	inflow balk velocity at jet inlet
$\mathbf{x} = (x, y, z)$	Cartesian coordinates

Greeksymbols

Δx, Δy, Δz	computational grid size
$\mathbf{\Phi} = (\phi_1, \ldots, \phi_\alpha, \ldots, \phi_{N_\mathrm{S}})$	passive scalars computed by Lagrangian particle method
Γ_α	concentration of species α
γ_α	concentration fluctuation of species α
$\Gamma_{\alpha 0}$	initial concentration of reactant or maximum concentration of chemical product
ψ	passive scalar computed by LES
λ	Taylor microscale
ν	kinematic viscosity
Q_N	approximate deconvolution filter
τ_M	mixing timescale for mixing model
ξ	mixture fraction

Subscript indices	
$\alpha, \mathrm{A}, \mathrm{B}, \mathrm{P}$	related to ϕ_α or chemical species A, B, or P
mix	related to mixing model
rms	rms value of fluctuation
Superscript indices	
(n)	related to particle n
Overscript indices	
$-$	low-pass filtered value
$\sim$	approximately deconvoluted value by applying Q_N to low-pass filtered value
Other special symbols	
$\langle * \rangle$	mean value calculated by ensemble or time average
$\langle * \vert V_M^n \rangle$	mean value in mixing volume V_{M}^n for particle n

References

[1] R. O. Fox, Computational Models for Turbulent Reacting Flows, Cambridge Univ. Pr., 2003.

[2] U. Schumann, Large-eddy simulation of turbulent diffusion with chemical reactions in the convective boundary layer, Atmos. Environ. 23 (8) (1989) 1713–1727.

[3] R. I. Sykes, D. S. Henn, S. F. Parker, W. S. Lewellen, Large-eddy simulation of a turbulent reacting plume, Atmos. Environ. 26 (14) (1992) 2565–2574.

[4] T. Michioka, S. Komori, Large-eddy simulation of a turbulent reacting liquid flow, AIChE J. 50 (11) (2004) 2705–2720.

[5] R. W. Bilger, Conditional moment closure for turbulent reacting flow, Phys. Fluids A 5 (1993) 436.

[6] S. B. Pope, PDF methods for turbulent reactive flows, Prog. Energy Combust. Sci. 11 (2) (1985) 119–192.

[7] D. C. Haworth, Progress in probability density function methods for turbulent reacting flows, Prog. Energy Combust. Sci. 36 (2) (2010) 168–259.

[8] J. Smagorinsky, General circulation experiments with the primitive equations: I. the basic experiment, Mon. Weather Rev. 91 (3) (1963) 99–164.

[9] M. Germano, U. Piomelli, P. Moin, W. H. Cabot, A dynamic subgrid-scale eddy viscosity model, Phys. Fluids A 3 (7) (1991) 1760–1765.

[10] P. Moin, K. Squires, W. Cabot, S. Lee, A dynamic subgrid-scale model for compressible turbulence and scalar transport, Phys. Fluids A 3 (11) (1991) 2746–2757.

[11] O. Métais, M. Lesieur, Spectral large-eddy simulation of isotropic and stably stratified turbulence, J. Fluid Mech. 239 (1992) 157–194.

[12] J. Bardino, Improved turbulence models based on large eddy simulation of homogeneous, incompressible turbulent flows, Ph.D. thesis, Department of Mechanical Engineering, Stanford University, Stanford, CA.

[13] S. Stolz, N. A. Adams, An approximate deconvolution procedure for large-eddy simulation, Phys. Fluids 11 (7) (1999) 1699–1701.

[14] S. Stolz, N. A. Adams, L. Kleiser, An approximate deconvolution model for large-eddy simulation with application to incompressible wall-bounded flows, Phys. Fluids 13 (4) (2001) 997–1015.

[15] S. Stolz, N. A. Adams, L. Kleiser, The approximate deconvolution model for large-eddy simulations of compressible flows and its application to shock-turbulent-boundary-layer interaction, Phys. Fluids 13 (10) (2001) 2985–3001.

[16] P. Schlatter, S. Stolz, L. Kleiser, LES of transitional flows using the approximate deconvolution model, Int. J. Heat Fluid Flow 25 (3) (2004) 549–558.

[17] W. Aniszewski, A. Bogusławski, M. Marek, A. Tyliszczak, A new approach to sub-grid surface tension for LES of two-phase flows, J. Comput. Phys. 231 (21) (2012) 7368–7397.

[18] C. Le Ribault, S. Sarkar, S. A. Stanley, Large eddy simulation of a plane jet, Phys. Fluids 11 (10) (1999) 3069–3083.

[19] C. B. da Silva, J. C. R. Hunt, I. Eames, J. Westerweel, Interfacial layers between regions of different turbulence intensity, Annu. Rev. Fluid Mech. 46 (2014) 567–590.

[20] C. B. da Silva, The behavior of subgrid-scale models near the turbulent/nonturbulent interface in jets, Phys. Fluids 21 (8) (2009) 081702.

[21] C. Bogey, C. Bailly, Decrease of the effective Reynolds number with eddy-viscosity subgrid modeling, AIAA J. 43 (2) (2005) 437–439.

[22] J. A. Domaradzki, N. A. Adams, Direct modelling of subgrid scales of turbulence in large eddy simulations, J. Turbulence 3 (24) (2002) 1.

[23] J. C. Hill, Homogeneous turbulent mixing with chemical reaction, Annu. Rev. Fluid Mech. 8 (1976) 135–161.

[24] P. J. Colucci, F. A. Jaberi, P. Givi, S. B. Pope, Filtered density function for large eddy simulation of turbulent reacting flows, Phys. Fluids 10 (1998) 499.

[25] Z. Warhaft, J. L. Lumley, An experimental study of the decay of temperature fluctuations in grid-generated turbulence, J. Fluid Mech. 88 (4) (1978) 659–684.

[26] P. K. Yeung, S. Xu, K. R. Sreenivasan, Schmidt number effects on turbulent transport with uniform mean scalar gradient, Phys. Fluids 14 (12) (2002) 4178–4191.

[27] T. Watanabe, Y. Sakai, K. Nagata, O. Terashima, H. Suzuki, T. Hayase, Y. Ito, Visualization of turbulent reactive jet by using direct numerical simulation, Int. J. Model. Simul. Sci. Comput. 4 (2013) 1341001.

[28] T. Watanabe, Y. Sakai, K. Nagata, Y. Ito, T. Hayase, Reactive scalar field near the turbulent/non-turbulent interface in a planar jet with a second-order chemical reaction, Phys. Fluids 26 (10) (2014) 105111.

[29] W. J. Layton, L. G. Rebholz, Approximate Deconvolution Models of Turbulence: Analysis, Phenomenology and Numerical Analysis, Springer-Verlag, Heidelberg, 2012.

[30] J. Mathew, R. Lechner, H. Foysi, J. Sesterhenn, R. Friedrich, An explicit filtering method for large eddy simulation of compressible flows, Phys. Fluids 15 (8) (2003) 2279–2289.

[31] S. Komori, K. Nagata, Effects of molecular diffusivities on counter-gradient scalar and momentum transfer in strongly stable stratification, Journal of Fluid Mechanics 326 (1996) 205–237.

[32] R. O. Fox, J. Villermaux, Unsteady-state IEM model: numerical simulation and multiple-scale perturbation analysis near perfect-micromixing limit, Chem. Eng. Sci. 45 (2) (1990) 373–386.

[33] C. Bogey, C. Bailly, Turbulence and energy budget in a self-preserving round jet: direct evaluation using large eddy simulation, J. Fluid Mech. 627 (2009) 129–160.

[34] C. Jiménez, F. Ducros, B. Cuenot, B. Bédat, Subgrid scale variance and dissipation of a scalar field in large eddy simulations, Phys. Fluids 13 (6) (2001) 1748–1754.

[35] C. D. Pierce, P. Moin, A dynamic model for subgrid-scale variance and dissipation rate of a conserved scalar, Phys. Fluids 10 (1998) 3041.

[36] A. W. Cook, W. K. Bushe, A subgrid-scale model for the scalar dissipation rate in nonpremixed combustion, Phys. Fluids 11 (1999) 746.

[37] M. J. Cleary, A. Y. Klimenko, A generalised multiple mapping conditioning approach for turbulent combustion, Flow, Turbul. Combust. 82 (4) (2009) 477–491.

[38] R. L. Curl, Dispersed phase mixing: I. Theory and effects in simple reactors, AIChE J. 9 (2) (1963) 175–181.

[39] S. M. Correa, A direct comparison of pair-exchange and IEM models in premixed combustion, Combust. Flame 103 (3) (1995) 194–206.

[40] S. Mitarai, J. J. Riley, G. Kosaly, Testing of mixing models for Monte Carlo probability density function simulations, Phys. Fluids 17 (4) (2005) 047101.

[41] T. Watanabe, Y. Sakai, K. Nagata, Y. Ito, T. Hayase, Enstrophy and passive scalar transport near the turbulent/non-turbulent interface in a turbulent planar jet flow, Phys. Fluids 26 (10) (2014) 105103.

[42] T. Watanabe, Y. Sakai, K. Nagata, O. Terashima, T. Kubo, Simultaneous measurements of reactive scalar and velocity in a planar liquid jet with a second-order chemical reaction, Exp. Fluids 53 (5) (2012) 1369–1383.

[43] T. Watanabe, Y. Sakai, K. Nagata, O. Terashima, Turbulent Schmidt number and eddy diffusivity change with a chemical reaction, J. Fluid Mech. 754 (2014) 98–121.

[44] T. Watanabe, Y. Sakai, K. Nagata, O. Terashima, Experimental study on the reaction rate of a second-order chemical reaction in a planar liquid jet, AIChE J. 60 (11) (2014) 3969–3988.

[45] H. Abe, H. Kawamura, Y. Matsuo, Direct numerical simulation of a fully developed turbulent channel flow with respect to the Reynolds number dependence, ASME J. Fluids Eng. 123 (2) (2001) 382–393.

[46] R. W. Bilger, L. R. Saetran, L. V. Krishnamoorthy, Reaction in a scalar mixing layer, J. Fluid Mech. 233 (1991) 211–242.

[47] Y. Morinishi, T. S. Lund, O. V. Vasilyev, P. Moin, Fully conservative higher order finite difference schemes for incompressible flow, J. Comput. Phys. 143 (1) (1998) 90–124.

[48] P. R. Spalart, R. D. Moser, M. M. Rogers, Spectral methods for the Navier-Stokes equations with one infinite and two periodic directions, J. Comput. Phys. 96 (2) (1991) 297–324.

[49] Y. Dai, T. Kobayashi, N. Taniguchi, Large eddy simulation of plane turbulent jet flow using a new outflow velocity boundary condition, JSME Int. J., Ser. B 37 (2) (1994) 242–253.

[50] C. B. da Silva, D. C. Lopesa, V. Raman, The effect of subgrid-scale models on the entrainment of a passive scalar in a turbulent planar jet, J. Turbulence 1 (2015) 1.

[51] S. B. Pope, Turbulent Flows, Cambridge Univ. Pr., 2000.

[52] M. Klein, A. Sadiki, J. Janicka, A digital filter based generation of inflow data for spatially developing direct numerical or large eddy simulations, J. Comput. Phys. 186 (2) (2003) 652–665.